

Renormalization group flow, competing phases, and the structure of superconducting gap in multi-band models of Iron based superconductors

Saurabh Maiti, Andrey V. Chubukov

Department of Physics, University of Wisconsin, Madison, Wisconsin 53706, USA

(Dated: April 12, 2019)

We perform an analytical renormalization group (RG) study to address the role of Coulomb repulsion, the competition between extended s-wave superconducting order ($s\pm$) and the spin density wave (SDW) order and the angular dependence of the superconducting gap in multi-pocket models of Iron based superconductors. Previous analytic RG studies considered a toy model of one hole and one electron pocket. We consider more realistic models of two electron pockets and either two or three hole pockets, and also incorporate the angular dependence of interaction. We neglect for simplicity one of the two hole pockets centered at $k = 0$, which is less nested with electron pockets, i.e., consider 3-pocket and 4-pocket models. In a toy 2-pocket model, SDW order always wins over $s\pm$ order at perfect nesting, and $s\pm$ order only appears at a finite doping, and only if RG flow extends long enough to overcome intra-pocket Coulomb repulsion. For multi-pocket models, we find two new effects. First, there always exists an attractive component of the interaction in $s\pm$ channel, such that the system necessary becomes a superconductor once it overcomes the competition from the SDW state. Second, in 3-pocket case (but not in 4-pocket case), there are situations when $s\pm$ order wins over SDW order even for perfect nesting, suggesting that SDW order is not a necessary pre-condition for the $s\pm$ order. Our results are in good agreement with recent numerical functional RG studies by Thomale et al. [arXiv:1002.3599v1]

I. INTRODUCTION

Since 2008 a lot of efforts in condensed-matter community have been devoted to solve the puzzle of high- T_c superconductivity (SC) in newly discovered Fe-based superconductors. To a large extent, in two years the community managed to obtain the data for the pnictides in the amount comparable to that collected for the cuprates over twenty years.

The family of Fe-based superconductors is already large and keeps growing. It includes doped 1111 systems $RFeAsO$ (R = Rare earth element)¹⁻⁴, doped 122 systems XFe_2As_2 (X =alkaline earth metals)⁵⁻⁷, as well as 111 and 11 systems like $LiFeAs$ ⁸ and $FeTe/Se$ ⁹. The parent compounds of most of these materials exhibit a spin density wave (SDW) order¹⁰, and superconductivity emerges upon either hole or electron doping, or upon gradual substitution of one pnictide by the other (As by P). In some systems, like $LiFeAs$ ⁸ and $LaFePO$ ¹¹, SC was found already without doping, instead of a magnetically ordered state.

ARPES¹², de-Haas van Alphen oscillations measurements¹³, and first-principle calculations¹⁴⁻¹⁶ all show that low-energy electronic structure of pnictides in 2D basal plane consists of two nearly circular, non-equivalent hole pockets located at the center of the Brillouin zone (BZ), and two symmetry-related elliptical electron pockets, located near the corners of the BZ in the folded zone scheme, or near $(0, \pi)$ and $(\pi, 0)$ points, respectively, in the unfolded zone scheme. [Folded and unfolded zones differ in treating the pnictides – folded zone takes into account the fact that there are two non-equivalent positions of pnictides above and below Fe plane, and has two Fe atoms in the unit cell, while unfolded zone incorporates only Fe atoms and has one Fe atom in the

unit cell.] These hole and electron pockets form warped cylinders in 3D space. In addition, in some pnictides (P-based)¹⁷, there is a fifth cylindrical hole pocket centered at (π, π) in the unfolded zone (at $(0, 0)$ in the folded zone, like other two hole pockets), while in other pnictides this fifth Fermi surface (FS) becomes a 3D sphere centered near $k_z = \pi$ along z -direction.

Apart from the electronic structure, a lot of work has been done over the last two years regarding the symmetry of the order parameter and the interplay between SDW and SC orders. Most of researchers (but not all, see Ref. 18) believe that the gap symmetry is extended s -wave ($s\pm$), meaning the gap transforms according to A_{1g} representation of D_{4h} tetragonal symmetry group, but the average gap values along hole and electron Fermi surfaces have different sign. However, the structure of the gap is still a puzzle. Early works based on either spin-fluctuation scenario^{16,19,20} or on renormalization group (RG) study of a toy model of one hole and one electron FS^{21,22} found a simple angle-independent $s\pm$ gap. Subsequent more sophisticated numerical studies, which take into account multi-orbital nature of low-energy excitations in the pnictides, have reported angular dependence of the $s\pm$ gap, with $\cos 2\phi$ variations on the electron FSs and $\cos 4\phi$ variations along the hole FSs^{17,23-26}. Analytically as well there are works incorporating the presence of the $\cos 2\phi$ modulations of the $s\pm$ gap on the electron FSs²⁷. If $\cos 2\phi$ variation is strong enough, the gap has “accidental” nodes along electron FSs, still preserving $s\pm$ symmetry. Another theory proposal includes $s\pm$ state with nodes on hole FSs due to strong $\cos 4\phi$ modulations²⁸, nodes at particular k_z along z -direction²⁹. Experiments are generally consistent with $s\pm$ gap symmetry, but whether or not the gap has nodes in particular materials is still subject of debate³⁰⁻³⁸. In addition, there

is no information yet from the experiments where the gap nodes are located, if present. ARPES³⁹ measurements of the gap along hole FSs (taken at fixed k_z) seem to indicate that the gap is almost angle independent, but the measurements of the gap along each of the two electron FSs are still lacking.

From theoretical perspective, the most relevant issue is the nature of the pairing interaction. Conventional electron-phonon coupling is always a candidate, particularly when the gap has s -wave symmetry, but has been shown to be rather weak¹⁵, and is incapable to account for $T_c \sim 50K$ even if one neglects destructive effect of Coulomb interaction. This leaves electron-electron interaction (i.e., Coulomb repulsion at a finite momentum transfer) as the dominant pairing interaction. Such interaction cannot give rise to a constant s -wave gap, but it can give rise to either momentum-dependent sign reversing gap along a given FS or two gaps of different signs along different FSs. Coulomb interaction at large momentum transfer can contribute to the pairing either directly, i.e., already at first order, or by renormalization of the interaction in spin/charge channel. In the latter case, it is customary to view the attractive interaction as being mediated by collective bosonic spin or charge excitations. The close proximity to magnetism makes spin fluctuations a preferable candidate^{16,20,23}, although orbital fluctuations were also considered recently⁴⁰. Both direct Coulomb interaction (the pair hopping) and magnetically-mediated interaction are attractive for $s\pm$ gap, and the total attractive pairing interaction is a combination of the two. However, to give rise to a pairing, this combined attractive pairing interaction has to overcome repulsion coming from Coulomb interaction at small momentum transfers. A conventional reasoning why Coulomb interaction is not an ultimate obstacle for s -wave superconductivity is McMillan-Tolmachev downturn renormalization of the repulsive Coulomb interaction, due to renormalizations in the same Cooper channel⁴¹. This argument works for phonon superconductors, but it does not work for electronic mechanism of superconductivity because both repulsive and attractive parts of the interaction renormalize in the same way, and McMillan-Tolmachev renormalization just reduces the strength of the repulsive interaction, but cannot change its sign.

How to overcome Coulomb interaction became the major issue for s -wave pairing in the pnictides. The situation is further complicated by the fact that the low-energy excitations are composed of all 5 hybridized Fe 3d-orbitals, and Coulomb interactions between fermions belonging to a given orbital and belonging to different orbitals are equally important. Only if all of these interactions are approximated by the same momentum-independent Hubbard U , this U cancels out in the pairing problem and one is left with a pure spin-mediated interaction (this was termed “Coulomb avoidance”⁴²). In reality, Coulomb interaction at small momentum transfer is larger than that at large momentum transfer, and

the intra-orbital and inter-orbital interactions are also different. As a result, bare Coulomb pairing interaction for superconductivity with angle-independent plus-minus gap is repulsive. Spin-mediated interaction is still attractive, but it is generally smaller than Coulomb repulsion, even when magnetic correlation length diverges (spin-mediated interaction only diverges at zero frequency, but for pairing one needs this interaction at finite frequencies, where it remains finite).

There are two possibilities to obtain $s\pm$ superconductivity despite strong Coulomb repulsion. First, multi-orbital character of excitations in the pnictides implies that the attractive pairing interaction (either pair hopping or spin-fluctuation exchange) is angle-dependent. The angle-dependence comes from coherent factors which dress up the interactions when one transforms from the orbital picture -in which different parts of the Fermi surface are made of different orbitals- to the band picture, in which free-fermion part is simply $\epsilon_k c_k^\dagger c_k$, and all information about multi-orbital character is passed onto interactions. Once interaction is angle-dependent, the gap also becomes angle-dependent, and the system adjusts the angle-dependence of the gap to minimize the effect of Coulomb repulsion (we discuss this in more detail below). The most natural is the case when the gap acquires $\pm \cos 2\phi$ components along the two electron FSs, and the magnitude of this component is adjusted to balance the interplay between short-range Coulomb repulsion and attractive interaction in $s\pm$ channel. When Coulomb repulsion dominates, the angle-dependent part is large, and the gap has four nodes along each of the electron FSs. This is most common result of RPA-type studies of the 2D pairing in the pnictides²³.

Second, one can analyze how the interactions evolve as the system flows towards smaller energies, relevant to superconductivity. This flow involves renormalizations of interactions in both particle-hole(p-h) and particle-particle(p-p) channel, and goes beyond RPA. This flow has been studied numerically, using functional renormalization group (fRG) technique²⁴⁻²⁶ and analytically^{21,27,43}, within parquet RG, justified by near-nesting. Both are weak-coupling studies, based on the Hamiltonian which contains screened Coulomb interaction, but no spin-fluctuation interaction. The results of both types of studies are quite similar: it turns out that, while Coulomb repulsion at small momentum transfer decreases upon system flow to smaller energies, the pair-hopping actually increases. The increase of the pair hopping is the result of the “push” from the inter-pocket density-density interaction which by itself leads to SDW instability. If RG flow of the couplings persists over a wide enough range of energies, pair-hopping interaction exceeds Coulomb repulsion, and the system develops an attraction in the $s\pm$ channel. In this situation, the $\pm \cos 2\phi$ variations of the gap on electron FSs induced by angle dependence of the interaction, are not overly relevant, and the system can develop an $s\pm$ gap without nodes.

While this scenario is quite generic, the earlier parquet RG study^{21,43} was more limited in scope. It was done for a toy model of one hole and one electron FS. For such a model, angle dependence of the interaction, by symmetry, can only be $\cos 4\phi$, $\cos 8\phi$, etc, which are subleading terms in the expansion of A_{1g} gap for a single FS. Such terms are generally irrelevant and were neglected in toy model analysis, i.e. the gap along each of the FS was approximated by a constant. As a result, there was nothing to adjust, and SC channel remained repulsive without RG. The RG flow did show that $s\pm$ interaction changes sign somewhere along the flow and becomes attractive. However, all along parquet RG flow, this interaction remains secondary to the interaction in the SDW channel. As a result, for perfect nesting the system develops an SDW order. Only when the system is doped and the logarithmical flow of the SDW vertex is cut at low energies ($\sim E_b$, which characterizes the scale associated with breaking of nesting), SC channel takes over and the system develops an s^{+-} superconductivity.

In the present paper we extend earlier parquet RG analysis to multi-pocket models of Fe-pnictides. We consider two models. The first one has two electron FSs, located at $(0, \pi)$ and $(\pi, 0)$ in the unfolded zone, and two hole FSs located near $(0, 0)$. The second model has an additional hole pocket centered at (π, π) in the folded zone. The presence or absence of this additional FS in different Fe-pnictides is attributed^{20,26} to the difference in the distance between the pnictide (e.g., As or P) and the Fe-plane. For simplicity, we keep one of the two hole FSs centered at $(0, 0)$, assuming that the other one is much less nested with electron FSs. Accordingly, our two models are 3-pocket and 4-pocket models. Throughout the paper we assume that all FSs are cylindrical and neglect their variations along k_z .

We argue that new physics emerges once one extends the model from 2 to 3 pocket, but 2 and 4 pocket models show qualitatively similar behavior. This result is consistent with early assertions^{21,27} that the 3-pocket model is the minimum model needed to understand the different physics of Fe -pnictides. It is also consistent with recent fRG study by Thomale *et al* (Ref.26).

We extend previous 2-pocket study in two directions. First, we incorporate the angular dependence of the interaction which gives rise to $\pm \cos 2\phi$ modulations of the gaps on electron FSs. In this situation, there are two different effective vertices for $s\pm$ gap symmetry, and we argue that one of them remains attractive over the entire RG flow, while the second changes sign and becomes attractive somewhere along RG flow but eventually becomes repulsive. There are also two SDW vertices of which only one is attractive along RG trajectory. We show that the stronger is the angular dependence of the interaction, the stronger is the tendency to develop an nodal $s\pm$ order.

Second, we re-analyze the interplay between SC and SDW channels. We show that in 3-pocket model, the trajectories of SC vertices are steeper than those of SDW

vertices, and the leading SC vertex is smaller than the leading SDW vertex only down to some RG scale. At smaller scales (i.e., when RG flow extends further to lower energies) the SC vertex overshadows SDW vertex even at perfect nesting. This effect has been recently observed in fRG study by Thomale *et al.*²⁶ for a model with 2 hole and 2 electron FSs (equivalent to our 3-pocket model, as, we recall, we neglect one of the hole FSs). Our analytical results agree with this study. We argue, based on our analytic consideration, that the crossing between SC and SDW vertices under RG flow is to a large extent a combinatoric effect – compared to 2-pocket case (where SDW and SC vertices flow to the same value under RG), the presence of the two electron FSs adds the factor of 2 to the renormalization of the SC vertex as the pair hopping can, e.g., hop a pair of $k, -k$ fermions from the hole FS to each of the two electron FSs, but momentum conservation does not allow such factor of 2 to appear in the renormalization of the SDW vertex.

Thomale *et al.* further argued that the crossing between SDW and SC vertex is not discernable once one includes an additional hole pocket at (π, π) . This corresponds to our 4-pocket model. Our analytical results show the same behavior. In fact, in our case we can explicitly show that SC and SDW vertices the vertices flow to the same value at the fixed point.

The rest of the paper is organized as follows: Section II outlines our approach, explains the subtleties in the RG flow, and discusses the technique by which we incorporate the momentum dependence into our analysis. In Sec. III we briefly review the results for the 2-pocket case. Section IV is the central section in the paper – here we discuss in detail SC vertices in the presence of angular dependence of the interaction, the RG flow, and the competition between SC and SDW instabilities for the 3-pocket model. In Sec. V we discuss 4-pocket model and argue that its behavior to a large extent is similar to that in 2-pocket model. We summarize our observations in the Conclusion.

II. DISCUSSIONS

Before starting the detailed description of each model, we present a brief discussion on the outline of our approach. We split this section into the following: the first describing the central idea behind our analysis and the second describing the technique through which we incorporate the angular dependence and finish by discussing the RG equations with angular dependence.

A. Approach

We consider 4-fermion interactions between fermions located close to the FSs of two or more pockets. We form a Hamiltonian with all possible quartic interactions

allowed by symmetry and ask what can be said about the onset of SC, SDW, and, possibly, CDW instabilities. The usual approach is to write down equations for effective vertices whose divergencies signal instabilities in particular channels and check for the existence of a solution for the critical temperature at which these vertices diverge. In case of competing instabilities, the equations for the effective vertices are in general coupled and, once the coupled system is solved, the instability with the highest T_c takes over.

As we said in the Introduction, when one does such an analysis, one deals with interactions taken at the scale of T_c , which are not the same as the terms in the Hamiltonian. To account for the flow of the couplings from the scale of the bandwidth down to T_c , we need RG analysis. This analysis can be formally applied to any case when the couplings flow, but it assumes renormalizability of the theory, which can be rigorously justified only when the RG flow is logarithmical (i.e., interactions vary as functions of the logarithm of the running scale E). One well-known example of logarithmical RG flow is the renormalization in the particle-particle channel (Cooper renormalization). Another, specific to our case, is the renormalization in the particle-hole channel, involving intermediate fermions from hole and electron pockets. Because hole and electron dispersions are of opposite sign, such a renormalization also generates logarithmical dependence of the running energy and/or momentum.

The logarithmical renormalizations in the particle-particle and particle-hole channels are characterized by corresponding polarization bubbles. Let c describe a hole band centered at $k = 0$ and f describe an electron band centered at Q . For a perfect nesting, the dispersion $\varepsilon_c(k) = -\varepsilon_f(k + Q)$. The two logarithmically singular polarization bubbles are

$$\begin{aligned}
 \Pi_{pp}^{cc}(q, \Omega) &= \Pi_{pp}^{ff}(q, \Omega) \\
 &= \int \frac{d^2k \, d\omega}{(2\pi)^3} G^c(k, \omega) G^c(q - k, \Omega - \omega) \\
 &= \frac{m}{2\pi} L + \dots \\
 \Pi_{ph}^{cf}(q + Q, \Omega) &= \int \frac{d^2k \, d\omega}{(2\pi)^3} G^c(k, \omega) G^f(q + Q + k, \Omega + \omega) \\
 &= -\frac{m}{2\pi} L + \dots \\
 L &= \frac{1}{2} \ln \left(\frac{\Lambda}{E} \right)
 \end{aligned} \tag{1}$$

where the dots stand for non-logarithmic terms, $E = \max\{\Omega, v_F q\}$ and $E > E_F$, Λ is the upper cutoff of order bandwidth, and the propagators are given by $G^x = \frac{1}{i\omega - \varepsilon_k^x}$, x being c or f .

The RG study requires caution as the couplings flow differently for energy scales above E_F and below E_F . The reasoning is simple: logarithmical RG analysis requires that internal momenta in each diagram for vertex renormalization be larger than external momenta, which are

of order k_F . When typical internal energies are larger than E_F , internal momenta are larger than k_F , and vertex corrections in both particle-particle and particle-hole channel are logarithmic. This gives rise to parquet RG. When typical energies are smaller than E_F , the strength of the renormalization in the particular channel depends on the interplay between external momenta. When total incoming momenta is zero, renormalization in the particle-particle channel is still logarithmically singular, but in the renormalization of the particle-hole channel, the logarithm is cut by external E_F . Conversely, for the vertex with transferred momentum equal to the distance between hole and electron FSs, the renormalization in the particle-hole channel is still logarithmical, but in the renormalization in the particle-particle channel, the logarithm is now cut by external E_F . As a result, the renormalizations in the particle-particle and particle-hole channels are coupled at energies above E_F , but become decoupled at energies below E_F . At such small energies parquet RG equations are replaced by conventional ladder RG equations $d\Gamma_i/dl = \Gamma_i^2$, where $l = \log E_F/E$. Thus the flow of the couplings splits into the flow from the bandwidth down to E_F , where different vertices are all coupled, and the flow below E_F , where different vertices are decoupled (see Fig. 1). This reasoning is particularly important in our case, as in pnictides $E_F \sim 100 \text{ meV}$ is much smaller than the bandwidth, which is a few electron volts.

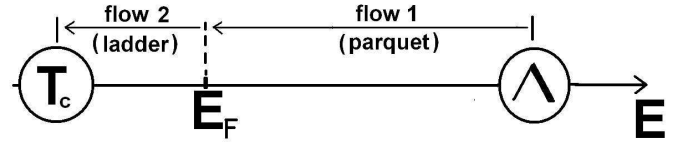


FIG. 1: Illustration showing how the couplings evolve under RG flow. The bare couplings (the parameters of the Hamiltonian) are defined at energies comparable to the bandwidth Λ . In pnictides, this scale is $2 - 3 \text{ eV}$, much larger than the Fermi energy $E_F \sim 0.1 \text{ eV}$. SC and SDW instabilities likely come from even smaller energies because instability temperatures are at least order of magnitude smaller than E_F . The couplings vary as one integrates out higher energies. This variation (i.e., the flow of the couplings from Λ down to the running scale E) can be generally captured by the RG technique. In pnictides, the flow is different above and below E_F . Above E_F , each of the couplings changes because of integrating out higher energy fermions in both particle-hole and particle-particle channels. The RG equations in this region are called parquet RG, because renormalizations extend in the two directions. Below E_F , each vertex continues to flow due to renormalizations in only one channel, either particle-hole or particle-particle, depending on the external momenta. The RG equations in this region are called ladder RG, because renormalizations extend only in one direction.

Depending on the character of the flow and the ratio of

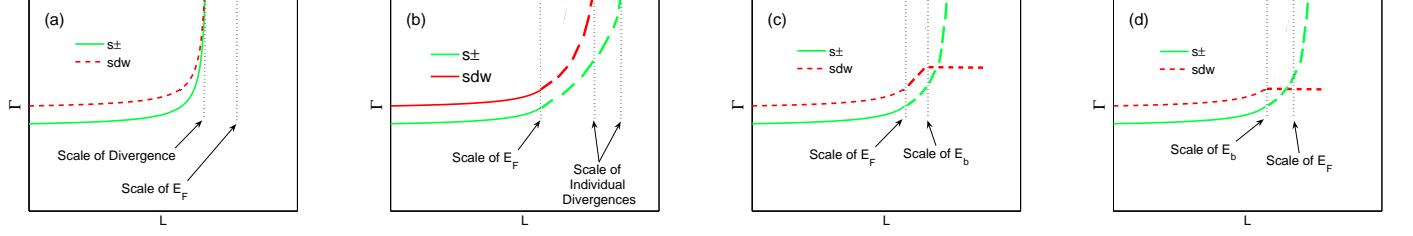


FIG. 2: Schematics of the RG flow of SC and SDW vertices Γ^{SDW} and $\Gamma^{s\pm}$. The horizontal scale is $L = \frac{1}{2}\ln\frac{\Lambda}{E}$ for $E > E_F$ and $\frac{1}{2}\ln\frac{\Lambda}{E_F} + \ln\frac{E_F}{E}$ for $E < E_F$. SC and SDW vertices remain coupled at energies larger than E_F but decouple below E_F . Depending on the bare values of the vertices, the ratio Λ/E_F , and the doping, four different scenarios are possible (panels (a)-(d)). For perfect nesting, there are two possibilities: (a) the vertices diverge at the same scale before the scale of E_F is reached. The ratio of the vertices not necessary tends to one, though. (b) E_F is reached before the vertices diverge. Then, below E_F , the vertices decouple, flow and diverge independently, each on its own scale. The vertex that had larger value at E_F diverges first and sets the instability. For non-perfect nesting (e.g., at a finite doping), SDW vertex eventually does not diverge. SC vertex still diverges, and the system becomes a SC even if SC instability was subleading at perfect nesting. The flow of the SDW vertex levels off either at $E_b < E_F$ (panel c), or at $E_b > E_F$ (panel d).

the bandwidth and the Fermi energy, several situations are possible and shown in Fig. 2:

- The RG flow diverges and the normal state becomes unstable before the scale of E_F is reached (Fig. 2a). In this situation, the instability comes from fermions with energies above E_F , and only parquet RG matters. This situation is the most interesting one from physics perspective as in all cases we study more than one vertex diverges at such a fixed point, and in several situations different vertices become equal at the fixed point which then has an enhanced symmetry (e.g., in the 2-band model, the vertices in SDW, SC, and orbital CDW channels diverge simultaneously within parquet RG, their ratio tends to one, and the fixed point has $O(6)$ symmetry⁴³). Unfortunately, this probably does not happen in the pnictides as otherwise the instability temperature would be larger than E_F , while in pnictides the largest instability T_{SDW} is only a fraction of E_F .
- The RG flow reaches E_F before couplings diverge (Fig. 2b). In this situation, parquet RG creates a hierarchy of the couplings at E_F : $\Gamma_i(E_F)$ (index i numbers the channels: SDW, SC, etc). Below E_F , different Γ_i decouple and, in the case of a perfect nesting, each continue evolving according to a ladder RG, i.e., like $\Gamma_i(E) = \Gamma_i(E_F)/(1 - \Gamma_i(E_F)\log\frac{E_F}{E})$. The instability occurs at the energy (temperature) at which $\Gamma_i(E_F)\log\frac{E_F}{E} = 1$. Obviously, the winning channel is the one in which the coupling is the largest at E_F .
- When nesting is not perfect, the coupling in the SC channel continues to follow $\Gamma^{SC}(E) = \Gamma^{SC}(E_F)/(1 - \Gamma^{SC}(E_F)\log\frac{E_F}{E})$ simply because SC instability involves pairs of fermions with \mathbf{k} and $-\mathbf{k}$ from the same FS and is insensitive to a deviation

from perfect nesting. However the logarithmic flow of SDW and CDW vertices is now cut at some scale E_b . Suppose $E_b < E_F$ (Fig. 2c). In this situation, SC eventually wins over SDW and CDW instabilities, even if superconducting Γ is subleading at E_F (but attractive).

- When E_b exceeds E_F (Fig. 2d) particle-hole and particle-particle channels decouple already within the applicability range of parquet RG. At $E < E_b$, SC vertex continue to grow as $\Gamma^{SC}(E) = \Gamma^{SC}(E_b)/(1 - \Gamma^{SC}(E_b)\log E_b/E)$, while vertices in density-wave channel get frozen at their values at $E \sim E_b$. In this situation, SC instability again wins, even if it was subleading at E_b , provided that the superconducting vertex is attractive at E_b .

A subtle point: below we will be presenting the RG flows of vertices and couplings at energies both above and below E_F in terms of the logarithmic variable $L \sim \log E$. One has to bear in mind, however, that the prefactor for the logarithm actually changes between $E > E_F$ and $E < E_F$ because for $E > E_F$ the integration over intermediate energies involves only positive excitations for electron states (and negative for hole state), i.e., $\int \frac{d^2k}{(2\pi)^2} = (m/2\pi) \int_E^\Lambda d\epsilon_k$, while for $E < E_F$, one has to linearize the dispersion of holes and electrons near the FS and integrate on both sides of E_F , i.e., $\int \frac{d^2k}{(2\pi)^2} = (m/\pi) \int_E^{E_F} d\epsilon_k$. To simplify the presentation we just define

$$L = \begin{cases} \frac{1}{2}\ln\frac{\Lambda}{E} & , E > E_F \\ \frac{1}{2}\ln\frac{\Lambda}{E_F} + \ln\frac{E_F}{E} & , E < E_F \end{cases}$$

and use the same symbol L for all energies. This is valid as long as we describe the system behavior at $E \gg E_F$ and $E \ll E_F$. The behavior in the crossover regime $E \sim E_F$ is more complex, but this is beyond the scope of the present paper. We will also use $L_{E_F} \equiv \frac{1}{2}\ln\frac{\Lambda}{E_F}$.

B. Incorporating angular dependence

As we said in the Introduction, multi-orbital character of low-energy excitations in Fe-pnictides implies that interactions between fermions located near hole or electron FSs depend on the angles along the FSs. To obtain angular dependence of various couplings from first principles, one has to transform from five-orbital to five-band picture and dress up Coulomb interactions by coherence factors. This has been done in several studies(see, e.g., Refs. 23,25,44), under the assumption that the Coulomb interaction is so strongly screened that it can be replaced by Hubbard U . This assumption is generally valid for systems with large FSs, because of many available particle-hole pairs for screening, but in systems with small FSs, like pnictides, much fewer number of particle-hole pairs are available, and the screening of Coulomb interaction is much weaker, and is actually a rather non-trivial phenomenon at small k_F . Because of this complication, the “first-principle” analysis of the angular dependence of the interaction is a rather difficult task.

One can, however, attempt to extract these angular dependence from symmetry considerations, similar to the one done for the cuprates. This is what we will do. Consider first the pairing vertex between fermions with incoming momenta k and $-k$ and outgoing momenta p and $-p$. Quite generally, for tetragonal D_{4h} symmetry group, this interaction can be divided into one- and two-dimensional representation, and one-dimensional representation can be further divided into A_{1g} , B_{1g} , B_{2g} , and A_{2g} harmonics, depending on the symmetry under the transformations under $k_{x,y} \rightarrow -k_{x,y}$ and $k_x \rightarrow k_y$. Basic functions from different representations do not mix, but each contains infinite number of components. s -wave pairing corresponds to fully symmetric A_{1g} representation. The pairing interaction within this approximation can be quite generally expressed as

$$u(k, p) = \sum_{m,n} A_{mn} \Psi_m(k) \Psi_n(p) \quad (2)$$

where $\Psi(k)$'s are the basis functions of the A_{1g} symmetry group - 1, $\cos k_x \cos k_y$, $\cos k_x + \cos k_y$, etc, and A_{mn} are coefficients. Suppose for definiteness that k belongs to hole FS and is close to $k = 0$. Expanding *any* wave function with A_{1g} symmetry near $k = 0$, one obtains, along $|\mathbf{k}| = k_F$,

$$\Psi_m(k) = a_m + b_m \cos 4\phi_k + c_m \cos 8\phi_k + \dots \quad (3)$$

If \mathbf{p} is near the same hole FS, the expansion of $\Psi_n(p)$ also involves $\cos 4\phi_p$, $\cos 8\phi_p$, etc. There are no fundamental reasons to expect that b_m , c_m , etc are much smaller than a_m , but sub-leading terms are often small numerically. Two examples are the numerical smallness of $\cos 6\phi$, etc components of the $d_{x^2-y^2}$ -wave gap in overdoped cuprates, compared to $\cos 2\phi$ gap, and the

smallness of $\cos 4\phi$, etc components of the gap along the hole FSs in the ARPES³⁹ data for the pnictides and in fRG²⁶ and RPA²³ calculations for 5-band Hubbard U models. Taking these examples as circumstantial evidence, we assume that $\cos 4\phi$, etc terms are small. If so, the interaction between fermions belonging to the hole FS can be approximated by angular-independent term.

The situation changes, however, when we consider pairing interaction between fermions belonging to different FSs. Suppose that k are still near the center of the Brillouin zone, but p are near one of the electron FSs, say the one centered at $(0, \pi)$. Consider all possible $\Psi_n(p)$ with A_{1g} symmetry. A simple experimentation with trigonometry shows that there are two different subsets of basic functions:

$$\begin{aligned} A : & 1, \cos p_x \cos p_y, \cos 2p_x + \cos 2p_y \dots \\ B : & \cos p_x + \cos p_y, \cos 3p_x + \cos 3p_y \dots \end{aligned} \quad (4)$$

Functions from class A have the same properties as before – they can be expanded in series of $\cos 4l\phi_p$ (l is integer). Functions from class B are different – they all vanish at $(0, \pi)$ and are expanded in series of $\cos(2\phi_p + 4l\phi_p)$ (i.e., the first term is $\cos 2\phi_p$, the second is $\cos 6\phi_p$, etc). Let's make the same approximation as before and neglect all terms with $l > 0$. The functions from class A can then be approximated by a constant, but the functions from class B are approximated by $\cos 2\phi_p$. As a result, the pairing interaction involving fermions from hole and one of the two electron FSs (labeled as e_1) has a generic form of

$$\begin{aligned} u_{e_1,h}(k, p) &= u_{e_1,h} + \bar{u}_{e_1,h} \cos 2\phi_{pe_1} + \dots \\ &= u_{e_1,h} (1 + 2\alpha \cos 2\phi_{pe_1}) + \dots \end{aligned} \quad (5)$$

where dots stand for $\cos 4\phi_k, \cos 4\phi_p, \cos 6\phi_p$, etc terms. 2 before the α is just for convenience for calculations. We emphasize that the constant term and the $\cos 2\phi_p$ term in (5) are the leading terms of the two subsets of interaction terms, each form series in $\cos 4\phi_{k,p}$. By the same reasoning, the interaction between fermions near two electron FSs centered at $(0, \pi)$ and $(\pi, 0)$ is expressed as

$$\begin{aligned} u_{e_1,e_2}(k, p) &\sim u_{e_1,e_2} (1 + 2\alpha \cos 2\phi_{ke_1} + \dots) \times \\ &\quad (1 + 2\alpha \cos 2\phi_{pe_2} + \dots) \end{aligned} \quad (6)$$

Observe also that the $\cos 2\phi$ terms in (5) and (6) change sign under the transformation $x \rightarrow y$ (like $d_{x^2-y^2}$ interaction in the cuprates), hence the prefactor for $\cos 2\phi_p$ term in (5) changes sign between the two electron FSs [$\cos 2\phi_{pe_1} \rightarrow -\cos 2\phi_{pe_2}$].

The pairing interaction in the form of Eq. (5) has been suggested in Ref. 27. These authors, however, didn't invoke multi-orbital structure of pnictides, in which case α scales as k_F^2 and is small when k_F is small. In fact, for

multi-orbital systems, coherent factors associated with the hybridization of 5 *Fe* bands are not small in k_F (Refs. 23,44), hence α *does not need to be small*. Accordingly, we will keep α as just a parameter marking the strength of angular dependence.

Once the pairing interaction has the form of Eqs. (5) and (6), the gap along hole FS is still angle-independent, but the gaps along the two electron FSs are in the form $\Delta_e \pm \bar{\Delta}_e \cos 2\phi$. When $\bar{\Delta}_e$ is small compared to Δ_e , we have nearly angle-independent gap, but when $|\bar{\Delta}_e| > |\Delta_e|$, the gap along electron FSs acquire the nodes at “accidental” values of ϕ .

C. Effect of Angular Dependence on RG analysis

The angle-dependence of the interaction is the key element of fRG approach, and this approach uses the full momentum dependence of the interactions, i.e., the full series of $\cos 4l\phi$ and $\cos(2\phi + 4l\phi)$ terms. At the same time, fRG approach assumes renormalizability (i.e., that the right-hand side of RG eqs contain only renormalized couplings, not some combinations of bare and renormalized couplings). In our analytical approach, we remain with logarithmic approximation in which case we explicitly preserve renormalizability.

We found, after explicitly evaluating the renormalizations of angle-dependent vertices, that the only way to justify RG procedure in this situation is to keep the angular dependence away from RG flow, i.e., in eq. 6, allow $u_{e1,e2}$, $u_{e1,h}$, and $u_{e2,h}$ to flow under RG, while α is kept unchanged. This is, in fact, how the interactions are decomposed in fRG studies^{25,26}. In our case this last approximation can be rigorously justified when α is small, and $u_{e1,e2}$ in Eq. (6) reduces to

$$u_{e1,e2}(k,p) \sim u_{e1,e2} (1 + 2\alpha (\cos 2\phi_{k_{e1}} + \cos 2\phi_{p_{e2}})) \quad (7)$$

We will keep α small in the RG calculations but will later assume without proof that the results of RG analysis are valid even when $\alpha \leq 1$. There are no new physical effects at $\alpha \leq 1$ compared to $\alpha \ll 1$, so the results at $\alpha \leq 1$ should be at least qualitatively correct by continuity.

As we said in the Introduction, the main goal of our analysis is to understand whether there are qualitative differences between RG flow and the pairing in 2, 3 and 4 pocket models for *Fe*-pnictides. We remind that we neglect -to simplify the analysis- one of two hole FSs around $k = 0$ (which has weaker nesting with electron FSs), so our 3 pocket model is essentially the simplified version of the original model with 4 pockets, and our 4 pocket model is the simplified version of the original model with 5 pockets. The next three sections deal with the comparison of 2,3, and 4-pocket models.

III. THE 2 POCKET MODEL

This has been studied before (Refs. 21,43) and we briefly review it here to set notations and for further comparisons with 3 and 4 pocket cases.

The 2 pocket model is a toy model consisting of one hole pocket in the center the folded Brillouin Zone (BZ), and four electron pockets at the corners as shown in Fig 3. To obtain parquet RG equations, we consider energies larger than E_F and E_b , at which deviations from perfect nesting become irrelevant. At such energies, we can set $E_F \rightarrow 0$ (and $E_B \rightarrow 0$) and take hole and electron dispersions to be just opposite in sign.

The interaction Hamiltonian for the 2-pocket model is (following earlier notation²¹)

$$\begin{aligned} \frac{m}{2\pi} H_{int} = & \sum u_1 c_{p_1 s}^\dagger f_{p_2 s'}^\dagger f_{p_4 s'} c_{p_3 s} + \sum u_2 c_{p_1 s}^\dagger f_{p_2 s'}^\dagger c_{p_4 s'} f_{p_3 s} + \sum \frac{u_3}{2} \left(c_{p_1 s}^\dagger c_{p_2 s'}^\dagger f_{p_4 s'} f_{p_3 s} + h.c. \right) \\ & + \sum \frac{u_4}{2} f_{p_1 s}^\dagger f_{p_2 s'}^\dagger f_{p_4 s'} f_{p_3 s} + \sum \frac{u_5}{2} c_{p_1 s}^\dagger c_{p_2 s'}^\dagger c_{p_4 s'} c_{p_3 s} \end{aligned} \quad (8)$$

where u_i are dimensionless couplings, and m is quasiparticle mass ($\varepsilon_f(k) = k^2/2m - \mu$). The sum is over the spin indices s and s' and the vector momenta p_1, p_2, p_3, p_4 with momentum conservation assumed. The c and f fermions reside at the hole and the electron bands respectively. We remind the reader that there is no angular dependence of the interactions here because the first angular term that comes in is 4ϕ , which we ignore in our approximation.

A. The Vertices

We begin by looking into the vertices in SC and SDW channels. For this, we introduce infinitesimally small SC and SDW order parameters Δ_{SC}^0 and Δ_{SDW}^0 , dress them up by including multiple interactions as shown diagrammatically in Fig. 4, and write the renormalized order parameters in the form

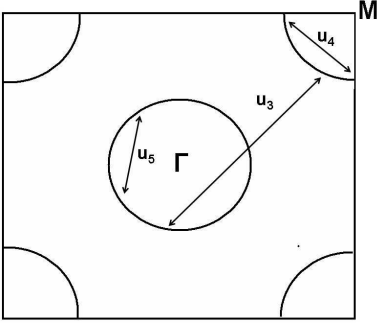


FIG. 3: Hole (center) and electron (corners) FSs in the folded BZ for 2-pocket model. The arrows with symbols indicate intra-pocket and inter-pocket pairing interactions (u_4 and u_5 are intra-pocket interactions, and u_3 is inter-pocket interaction). There also exist density-density and exchange interactions between hole and electron pockets (u_1 and u_2 terms, respectively, not shown).

$$\Delta_i = \Delta_i^0 (1 + \Gamma_i L) \quad (9)$$

For a given i , Δ_i becomes nonzero even for vanishing Δ_i^0 when the corresponding Γ_i diverges.

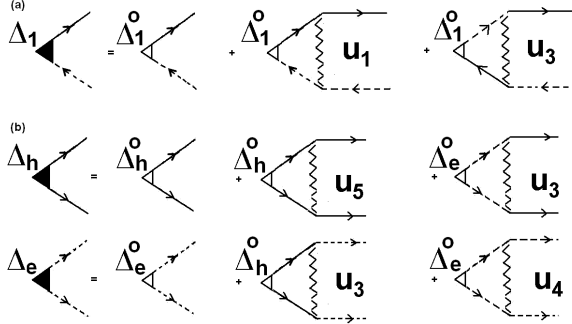


FIG. 4: Diagrams for the renormalization of infinitesimally small SDW and SC vertices, added to the Hamiltonian in order to calculate response functions. Unshaded triangles - bare vertices, shaded triangles - full vertices, wave lines - fully renormalized interactions. Solid lines correspond to c fermions and the dashed line to f fermions. Δ_1 is SDW vertex and Δ_h and Δ_e are SC vertices on hole and electron FSs.

The computations for the 2-pocket model is straightforward. For the SDW order parameter, we immediately obtain from Fig. 4, $\Gamma^{SDW} = u_1 + u_3$. For the SC channel, we obtain from Fig. 4

$$\begin{pmatrix} 1 - u_5 L & -u_3 L \\ -u_3 L & 1 - u_4 L \end{pmatrix} \begin{pmatrix} \Delta_h^0 \\ \Delta_e^0 \end{pmatrix} = \begin{pmatrix} \Delta_h \\ \Delta_e \end{pmatrix} \quad (10)$$

where $\Delta_{e,h}$ are order parameters on hole and electron FSs. Diagonalizing this set and casting the result in the form of Eq. (9), we obtain two SC Γ 's. One corresponds

to a conventional s -wave pairing, is repulsive for all positive u_i and is of no interest to us, another corresponds to $s \pm$ pairing and is given by

$$\Gamma^{s \pm} = \frac{-(u_4 + u_5) + \sqrt{(u_4 - u_5)^2 + 4u_3^2}}{2} \quad (11)$$

For $u_4 = u_5$, $\Gamma^{s \pm}$ reduces to $\Gamma^{s \pm} = -u_4 + u_3$.

The SDW vertex is attractive for positive u_1 and u_3 , while $\Gamma^{s \pm}$ is attractive only when inter-band pair hopping term exceeds intra-band repulsive interaction. Like we said, this is very unlikely because both interactions originate from Coulomb interaction, and screened Coulomb interaction at small momentum transfer (i.e., u_4 and u_5) is larger than that at large momentum transfer (i.e., u_3).

To understand whether the negative sign of $\Gamma^{s \pm}$ can be reversed, we need to consider RG flow of the couplings. This what we do next.

B. RG flow between Λ and E_F

The RG equations for the couplings have been obtained in²¹, and we just quote the result:

$$\begin{aligned} \dot{u}_4 &= -[u_4^2 + u_3^2] \\ \dot{u}_5 &= -[u_5^2 + u_3^2] \\ \dot{u}_1 &= [u_1^2 + u_3^2] \\ \dot{u}_2 &= [2u_1 u_2 - 2u_2^2] \\ \dot{u}_3 &= [4u_1 u_3 - 2u_2 u_3 - (u_4 + u_5)u_3] \end{aligned} \quad (12)$$

The derivative is with respect to L . These equations have a single non-trivial fixed point at which all couplings diverge and tend to $u_3 = \sqrt{5}u_1$, $u_4 = u_5 = -u_1$, $u_2 \propto (u_1)^{1/3}$. The flow of SDW and SC vertices is shown in Fig. 6a. In the process of RG flow, the SC vertex $\Gamma^{s \pm}$ changes sign and become attractive. The ratio $\Gamma^{s \pm} / \Gamma^{SDW}$ remains smaller than one during the flow, but tends to one upon approaching the fixed point, i.e., if this fixed point is reached, superconducting and SDW instabilities occur simultaneously, and the system actually cannot distinguish between the two. There is another vertex, which corresponds to a current CDW instability, which tends to the same value as SDW and SC vertices. The combination of 3-component SDW, 2-component SD and 1-component CDW instabilities makes the fixed point $O(6)$ symmetric.

The sign change of the superconducting $\Gamma^{s \pm}$ is the most notable effect within the parquet RG flow. Its physics originates in the effective “attraction” between SC and SDW fluctuations (not the order parameters!), what is reflected in the fact that u_3 , which is the attractive component of $\Gamma^{s \pm}$, gets a boost from u_1 , which contributes to Γ^{SDW} – the $4u_1 u_3$ term in the r.h.s. of the RG equation for \dot{u}_3 . This term overshadows the negative effect from u_2 , u_4 , and u_5 and gives rise to the increase of

u_3 under RG. At the same time, intra-pocket repulsions u_4 and u_5 decrease under RG. At some point, u_3 prevails and $\Gamma^{s\pm}$ becomes positive.

However, as we said earlier, parquet RG is only valid at energies above E_F . It is unlikely that the fixed point is reached above E_F , otherwise there would be at least pseudogap effects present above E_F , but there is no evidence for them in the pnictides. More likely, the couplings evolve under parquet RG (and $\Gamma^{s\pm}$ possibly changes sign at some scale), but u_i remain finite at E_F . To continue below this scale we need to derive a different set of equations, for which $u_i(E_F)$ serve as initial conditions.

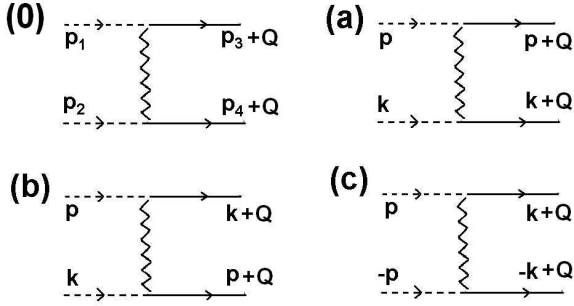


FIG. 5: (0) The u_3 vertex with general momenta p_1, p_2, p_3+Q, p_4+Q (all p_i are small and $p_1+p_2=p_3+p_4$). During calculations, three kinds of u_3 vertices arise—(a) the one with $p_1=p_3$, (b) the one with $p_2=p_3$, and (c) the one with $p_1+p_2=0$. The vertex ‘b’ contributes to the renormalization in p-h channel, and the vertex ‘c’ contributes to the renormalization in the p-p channel.

C. RG flow below the scale of E_F

The RG equations below E_F for 2-pocket model have been derived in Ref. 43 and we just quote the result. The most essential difference with the previous subsection concerns u_3 vertex, which contributes to both SC and SDW channels. Below E_F the structure of the external momenta becomes relevant, and one has to distinguish between $u_3^{(a)}$ with zero transferred momentum, $u_3^{(b)}$ with momentum transfer Q , and $u_3^{(c)}$ with zero total momentum (see Fig. Fig. 5). Each of the vertices now undergoes logarithmic renormalization in its own channel, crossed renormalizations no longer contribute because internal $E = O(E_F)$, and the arguments of the corresponding logarithms become $O(1)$. The new equations are

$$\begin{aligned}\dot{u}_3^{(a)} &= 2u_1u_3^{(a)} - 2u_2u_3^{(a)} \\ \dot{u}_3^{(b)} &= 2u_1u_3^{(b)} \\ \dot{u}_3^{(c)} &= -[u_4 + u_5]u_3^{(c)} \\ \dot{u}_4 &= -[u_4^2 + (u_3^{(c)})^2] \\ \dot{u}_5 &= -[u_5^2 + (u_3^{(c)})^2] \\ \dot{u}_1 &= [u_1^2 + (u_3^{(b)})^2] \\ \dot{u}_2 &= [2u_1u_2 - 2u_2^2]\end{aligned}\quad (13)$$

where the derivative is now with respect to $l = \log E_F/E$. The effective vertices in the SDW and SC channels also get modified and become

$$\begin{aligned}\Gamma^{SDW} &= u_1 + u_3^{(b)} \\ \Gamma^\pm &= \frac{-(u_4 + u_5) + \sqrt{(u_4 - u_5)^2 + 4(u_3^{(c)})^2}}{2}\end{aligned}\quad (14)$$

One can easily verify that new vertices satisfy

$$\frac{d\Gamma_i}{dL} = \Gamma_i^2 \quad (15)$$

as it should be because SC and SDW channels are now decoupled (no cross-terms in RG equations).

The behavior of the vertices below E_F is illustrated in Fig. 6 b,c. If SC vertex is already positive (attractive) at E_F (Fig. 6b), it diverges at some scale below E_F , but for perfect nesting SDW vertex diverges first. On doping, SDW vertex levels off, and the first instability eventually becomes an $s\pm$ state. If SC vertex remains negative at E_F (Fig. 6c), it decreases below E_F but still remains negative. In this situation, the system can only develop a SDW instability at perfect and near-perfect nesting.

To summarize: in a 2-pocket model three scenarios are possible: (i) the instability occurs simultaneously in SDW, SC, and CDW channels, and a fixed point has $O(6)$ symmetry, (ii) SDW instability wins at perfect nesting, but yields to $s\pm$ superconductivity upon doping, and (iii) SDW instability exists near perfect nesting, but no SC instability emerges when SDW order is suppressed by doping. For the cases (i) and (ii), the SC gap has a simple plus-minus form, i.e., the gaps along hole and electron FSs are angle independent (up to $\cos 4\phi$ terms which we neglected) and are of the opposite signs.

The 2-pocket model is indeed only a toy model for the pnictides. The actual band structure of the pnictides includes two electron FSs and at least two hole FSs. The question we now address is whether qualitatively new system behavior emerges when we increase the number of bands(pockets specifically). We argue below that there are new features not present in a 2-pocket model.

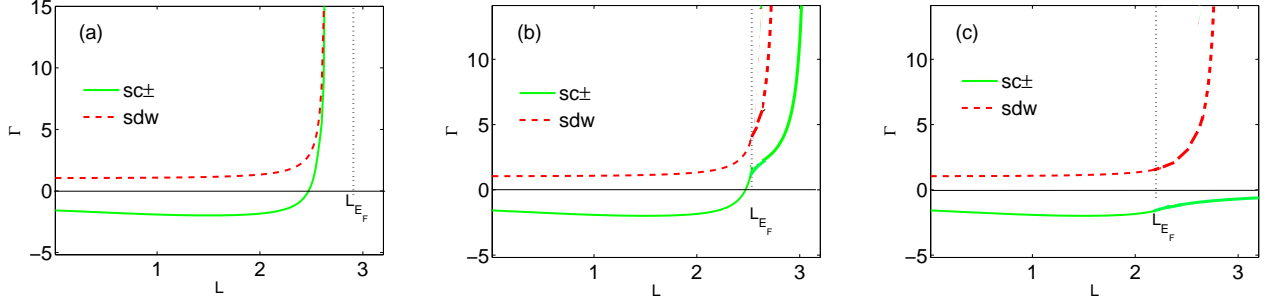


FIG. 6: Running vertices in SDW and SC $s\pm$ channel for the 2-pocket case at perfect nesting as functions of L . Three qualitatively different scenarios are possible: (a) vertices diverge before L_{E_F} is reached. Both vertices flow to the same fixed point, their ratio tends to one, and the fixed point has an extended symmetry. (b) L_{E_F} is reached before the fixed point, but in the range of L where the SC vertex is already attractive (positive). The vertices flow independent of each other beyond L_{E_F} (below E_F), the SDW vertex diverges first. On doping SDW yields to SC (see Fig. 2). (c) The value L_{E_F} is reached when SC vertex is still repulsive (negative). In this case SC instability does not occur even after SDW instability is eliminated by doping.

IV. 3 POCKET MODEL

As we just said, the FS of Fe-pnictides consists of two cylindrical electron FSs and either two or three cylindrical hole FSs, depending on the material. We neglect k_z variation of the FSs and consider a cross section in XY plane. The two electron FSs are ellipses, centered, in the unfolded zone, at $(0, \pi)$ and $(\pi, 0)$. Two hole FSs are circles centered at $(0, 0)$, and the third hole FS, if present, is located at (π, π) . The two FSs centered at $(0, 0)$ are of non-equal size, and one of them is less nested with

electron FSs than the other. Because one of our goals is to select the minimal model for the pnictides, we only include into consideration the hole FS at $(0, 0)$ which has stronger nesting with electron FSs and neglect the other one. This leaves either 3 or 4 FS pockets, depending on whether the hole FS at (π, π) is present or not.

We consider 3-pocket and 4-pocket models separately, and argue that most of the new physics shows up already in the 3-pocket model. We begin with the 3-pocket case.

The interaction Hamiltonian for the 3-pocket model is

$$\begin{aligned}
 \frac{m}{2\pi} H_{int} = & \sum u_1^{(1)} c_{p_1s}^\dagger f_{1p_2s'}^\dagger f_{1p_4s'} c_{p_3s} + \sum u_2^{(1)} c_{p_1s}^\dagger f_{1p_2s'}^\dagger c_{p_4s'} f_{1p_3s} + \sum \frac{u_3^{(1)}}{2} \left(c_{p_1s}^\dagger c_{p_2s'}^\dagger f_{1p_4s'} f_{1p_3s} + h.c. \right) \\
 & + f_1 \leftrightarrow f_2 \text{ and } u_i^{(1)} \leftrightarrow u_i^{(2)} \\
 & + \sum \frac{u_5}{2} c_{p_1s}^\dagger c_{p_2s'}^\dagger c_{p_4s'} c_{p_3s} + \sum \frac{u_4^{(1)}}{2} f_{1p_1s}^\dagger f_{1p_2s'}^\dagger f_{1p_4s'} f_{1p_3s} + \sum \frac{u_4^{(2)}}{2} f_{2p_1s}^\dagger f_{2p_2s'}^\dagger f_{2p_4s'} f_{2p_3s} \\
 & + \sum u_6 f_{1p_1s}^\dagger f_{2p_2s'}^\dagger f_{2p_4s'} f_{1p_3s} + \sum u_7 f_{1p_1s}^\dagger f_{2p_2s'}^\dagger f_{1p_4s'} f_{2p_3s} + \sum \frac{u_8}{2} \left(f_{1p_1s}^\dagger f_{1p_2s'}^\dagger f_{2p_4s'} f_{2p_3s} + h.c. \right)
 \end{aligned} \tag{16}$$

This is a straightforward generalization of the 2-pocket case (see also Ref. 45). The notations are the same as for the 2-pocket model, but now f_1 and f_2 refer to fermions from the two different electron bands. The new terms u_6, u_7 , and u_8 are different inter-pocket interactions between f -fermions. Because we now have two different sets of electron state, it is convenient to work in the unfolded BZ, and in Fig 7 we show the interactions in the unfolded BZ that contribute to the pairing vertex. There are, however, subtle effects related to the actual, As -induced differences between folded and unfolded zones,

and we will discuss them below.

The two electron bands are related by symmetry $k_x \leftrightarrow k_y$ (i.e., $\epsilon_{f_1}(k_x, k_y) = \epsilon_{f_2}(k_y, k_x)$), and it is natural to set $u_i^{(1)} = u_x^{(2)} = u_i$ (i runs between 1 and 4). We verified that no new terms are generated under RG flow, however the interactions between electron pockets must be included as they anyway are generated by RG.

The angular dependence of the vertices is incorporated in the same manner as described in Sec. II, by including $\alpha \cos 2\phi$ terms. To simplify calculations, we first neglect the angular dependence of the intra-pocket electron-

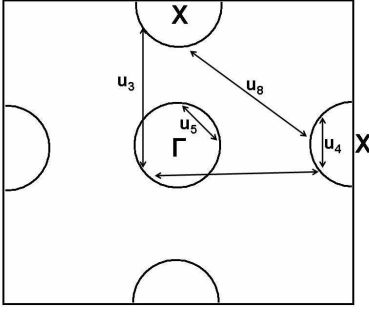


FIG. 7: Hole (center) and electron(edges) FSs in the unfolded BZ for 3-pocket model. The arrows with symbols indicate various intra-pocket and inter-pocket interactions which contribute to the SC vertex. There exist other density-density and exchange inter-pocket interactions (u_1 , u_2 , u_6 , and u_7 terms, not shown).

electron interaction u_4 . This is in line with our desire to treat intra-pocket interactions within hole and electron pockets on equal footing. Later we show that including angular dependence of u_4 will not change the results qualitatively.

A. The vertices

The computational procedure is the same as before. We introduce infinitesimally small SC and SDW vertices, dress them up by the interactions, and express the renormalized vertices in terms of the running couplings.

The diagrammatic expressions for the renormalized vertices are presented in Fig. 8. For the SDW vertex we choose the form $\Delta_1^{SDW} + \Delta_2^{SDW} \cos 2\phi$, ϕ being the angle on the electron FS. For SC vertex on hole FS it is Δ_h and for electron FSs it is $\Delta_e = \Delta_e + \bar{\Delta}_e \cos 2\phi$ for one FS and $\Delta_e = \Delta_e - \bar{\Delta}_e \cos 2\phi$ on the other as required by symmetry. If $|\bar{\Delta}_e| > |\Delta_e|$, the SC gap has nodes along the FS. The nodes are ‘accidental’ in the sense that they are not protected by any symmetry (unlike the d-wave counterpart).

For the SC vertex we then obtain the coupled set of equations

$$\begin{pmatrix} 1 - u_5 L & -2u_3 L & -2\alpha u_3 L \\ -u_3 L & 1 - \tilde{u}_4 L & 0 \\ -2\alpha u_3 L & 0 & 1 \end{pmatrix} \begin{pmatrix} \Delta_h^o \\ \Delta_e^o \\ \bar{\Delta}_e^o \end{pmatrix} = \begin{pmatrix} \Delta_h \\ \Delta_e \\ \bar{\Delta}_e \end{pmatrix} \quad (17)$$

where, $\tilde{u}_4 = u_4 + u_8$. For the SDW vertex $\Delta_{1,2}$ we get (assuming that $\Delta_{1,2}$ are real)

$$\begin{pmatrix} 1 + (u_1 + u_3)L & \frac{\alpha}{2}(u_1 + u_3)L \\ \alpha(u_1 + u_3)L & 1 \end{pmatrix} \begin{pmatrix} \Delta_1^o \\ \Delta_2^o \end{pmatrix} = \begin{pmatrix} \Delta_1 \\ \Delta_2 \end{pmatrix} \quad (18)$$

The effective vertices are found by diagonalizing these matrices and casting the results into the forms $\Delta_i = \Delta_i^o(1 + \Gamma_i L)$. For $\alpha = 0$, the formulas simplify and we

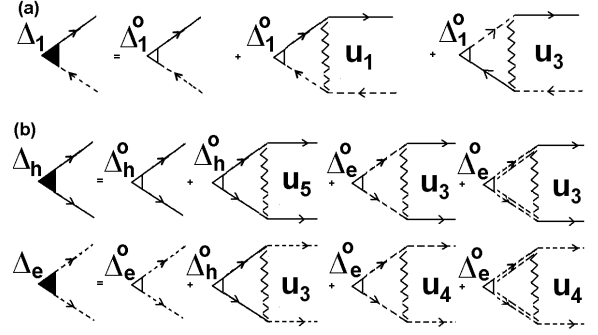


FIG. 8: The diagrams form the (a) density wave and (b) pairing vertices for the 3-pocket model. Notations are the same as in Fig. 4. Single and double dashed lines describe fermions from the two electron bands.

have one relevant SC and one relevant SDW vertices in the form

$$\begin{aligned} \Gamma^{s\pm} &= \frac{-(\tilde{u}_4 + u_5) + \sqrt{(\tilde{u}_4 - u_5)^2 + 8(u_3)^2}}{2} \\ \Gamma^{SDW} &= \Gamma_1^{SDW} = u_1 + u_3 \end{aligned} \quad (19)$$

Other vertices, when we look at the flow of the vertices, are either zero or definitely negative and hence irrelevant. At finite α , we obtain two Γ 's for the SDW vertex: $\Gamma_1^{SDW} = (u_1 + u_3)(1 + \sqrt{1 + 2\alpha^2})/2$ and $\Gamma_2^{SDW} = -(u_1 + u_3)(\sqrt{1 + 2\alpha^2} - 1)/2$. The second one is repulsive and irrelevant, the first one is attractive and leads to an SDW instability near perfect nesting. For the SC vertex, the three Γ_i^{SC} are obtained by solving the cubic equation. The analytical expressions are long and we refrain from presenting them (we will show all three Γ_i^{SC} in the figures). It is essential, however, that for *any* $\alpha \neq 0$, one of three Γ_i^{SC} is attractive even when $\tilde{u}_4 + u_5$ is larger than u_3 . For small α , this solution is

$$\Gamma_{new}^{s\pm} = \begin{cases} \alpha^2 \left[\frac{4u_3^2 u_5}{\tilde{u}_4 u_5 - 2u_3^2} \right] & , L < L_o \\ \Gamma^{s\pm} \left[1 + \alpha^2 \left(\frac{2u_3^2 (-\Delta u + \sqrt{(\Delta u)^2 + 8u_3^2})}{(\Gamma^{s\pm})^2 \sqrt{(\Delta u)^2 + 8u_3^2}} \right) \right] & , L > L_o \end{cases}$$

where $\Delta u = \tilde{u}_4 - u_5$ and $\Gamma^{s\pm}$ is given by Eq. 19. Let's recall that \tilde{u}_4 and u_5 are small momentum transfer coulomb components and for small renormalizations, these are positive and larger than u_3 , the large momentum component. Hence $\tilde{u}_4 u_5 - 2u_3^2$ is generally positive making the new branch positive (attractive). There is a certain scale (say L_o), where the old solution crosses the new induced solution. Beyond L_o , the solution passes to the old branch as we will demonstrate in a later subsection. We now proceed with the RG flow.

B. RG flow between Λ and E_F

Like in 2-pocket case, at $\Lambda > E > E_F$, renormalizations in p-h and p-p channels are logarithmical and independent of the location of external momenta. The derivation of parquet RG equations is straightforward but requires more efforts as there are new terms in the Hamiltonian. For illustration, we show in Fig 9 the diagrams contributing to the renormalization of the vertices u_4 and u_3 . The renormalization of other vertices proceeds in a similar fashion.

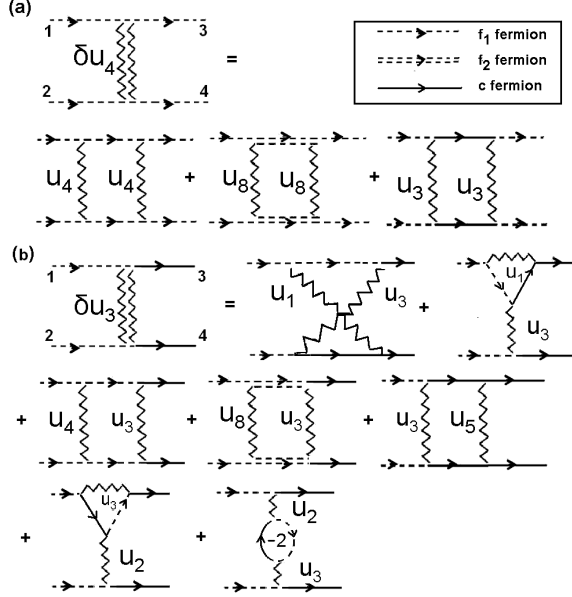


FIG. 9: Second order diagrams for the renormalizations of u_4 and u_3 vertices (panels a and b, respectively). The combinatorial factors are not shown but must indeed be included.

Collecting the diagrams for the renormalization of all couplings, we find that the terms u_6 and u_7 are decoupled from the rest of the terms and are renormalized as $\overline{u_6 \pm u_7} = -(u_6 \pm u_7)^2$, while the other six vertices are all coupled and flow according to

$$\begin{aligned} \dot{u}_5 &= -[u_5^2 + 2u_3^2] \\ \dot{u}_4 &= -[u_4^2 + u_8^2 + u_3^2] \\ \dot{u}_8 &= -[u_3^2 + 2u_8u_4] \\ \dot{u}_1 &= +[u_1^2 + u_3^2] \\ \dot{u}_2 &= +[2u_1u_2 - 2u_2^2] \\ \dot{u}_3 &= +[4u_1u_3 - 2u_2u_3 - u_5u_3 - (u_4 + u_8)u_3] \end{aligned} \quad (20)$$

Because u_6 and u_7 are not present in either SC or SDW vertices, we focus only on the set of six coupled RG equations, Eq. (20).

On a more careful look we also find that there are actually only five coupled equations: if we introduce $\tilde{u}_4 = u_4 + u_8$ and $u_8 - u_4$ instead of u_4 and u_8 , we immediately

find that only \tilde{u}_4 is coupled to other terms, while $u_8 - u_4$ is renormalized by itself, as

$$\overline{u_8 - u_4} = -(u_8 - u_4)^2 \quad (21)$$

Only \tilde{u}_4 appears in SC and SDW vertices, so we skip Eq. (21). We caution the readers, however, that the flow of, e.g., $u_8 - u_4$ depends on the bare value of this combination. If the bare value is positive, $u_8 - u_4$ flows to zero and is totally irrelevant. If, however, the bare value is negative, running $u_8 - u_4$ diverges at $|u_8 - u_4|_0 L$ where subindex 0 indicated bare value. This divergence leads to a competing instability. Throughout this paper we assume that the bare values of all u_i are such that no competing instability comes ahead of either SC or SDW instability, and focus on the rest of Eq. (20). Eliminating $u_8 - u_4$ from this set and introducing \tilde{u}_4 , we obtain

$$\begin{aligned} \dot{u}_5 &= -[u_5^2 + 2u_3^2] \\ \dot{\tilde{u}}_4 &= -[\tilde{u}_4^2 + 2u_3^2] \\ \dot{u}_1 &= +[u_1^2 + u_3^2] \\ \dot{u}_2 &= +[2u_1u_2 - 2u_2^2] \\ \dot{u}_3 &= +[4u_1u_3 - 2u_2u_3 - u_5u_3 - \tilde{u}_4u_3] \end{aligned} \quad (22)$$

This set of equations can be easily solved numerically. Fig 10 shows the plot of u_5/u_1 , \tilde{u}_4/u_1 , u_2/u_1 , and u_3/u_1 with L . For simplicity, we set bare values of \tilde{u}_4 and u_5 to be equal, the two then remain equal during the flow. The attainment of the fixed point is indicated by the dots. Like in 2-pocket model, intra-pocket repulsions \tilde{u}_4 and u_5 decrease under RG, change sign at some value of L , and become negative at larger L . This sign change (overscreening) goes beyond a conventional McMillan-Tolmachev screening of the Coulomb interaction is the result of the “push” from u_3 , which in turn increases under RG due to the “push” from u_1 which is the part of SDW vertex. So, eventually, overscreening is the result of the “attraction” between SDW and SC fluctuations.

We now substitute the running couplings into the expressions for SC and SDW vertices and check how they flow. The results are presented in Fig. 11. For the SDW vertices, the positive one increases with L , like in the 2-pocket model, while the negative one (the one induced by α become more negative, i.e., even less relevant in the process of RG flow. For the SC vertices one Γ^{SC} is positive for all L , other two are negative and hence irrelevant. The positive Γ^{SC} almost coincides with the solution induced by α at small L , and almost coincides with the solution which existed at $\alpha = 0$ at larger L . We emphasize that for all values of L this is the same solution, i.e., there is no level crossing (see Fig. 11).

In Fig. 12a we compare the behavior of Γ^{SDW} and Γ^{SC} as functions of L assuming that the fixed point is reached at energies above E_F . At small L , we have the same situation as in 2-pocket model: SDW vertex is larger than SC vertex. However, the rate of increase of the SC vertex

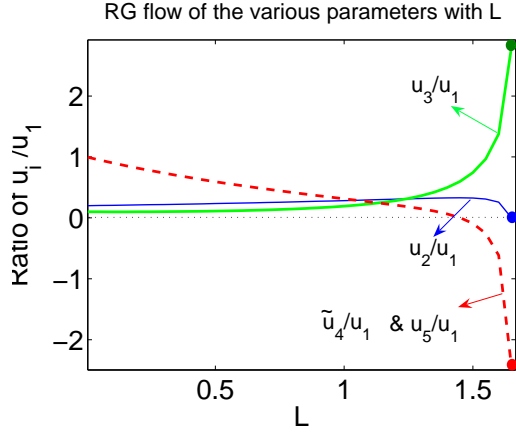


FIG. 10: The solution of Eq. (22) – the RG flow of u_5 , \tilde{u}_4 , u_2 , and u_3 (all relative to u_1) with L . For simplicity, we set bare values of \tilde{u}_4 and u_5 equal. Note how, as fixed point is approached, the renormalized Coulomb repulsion at small momenta (u_5 and \tilde{u}_4 terms) is suppressed and eventually changes sign, while the pair hopping term u_3 is strengthened.

exceeds that of the SDW vertex, and at some L before the fixed point is reached Γ^{SC} crosses Γ^{SDW} implying that the superconductivity becomes the leading instability even at perfect nesting. Such crossings has been reported in fRG calculations²⁶ for the same model. We view the agreement as a good indication that numerical fRG and analytical parquet RG approaches describe the same physics. In our analytical RG, the reason for the crossing is combinatoric: compared to 2-pocket case (where SDW and SC vertices flow to the same value under RG), the presence of the second electron FS adds the factor of 2 to the renormalization of the SC vertex as a pair of fermions from the hole FS can hop to each of the two electron FSs. However, there is no such factor of 2 in the renormalization of the SDW vertex due to momentum conservation.

The SC order parameter by itself has an interesting character. We recall that we approximate the gap along the hole FS by a constant Δ_h and approximate the gap along the two electron FSs by $\Delta_e \pm \tilde{\Delta}_e \cos 2\phi$. At small L , the attractive Γ^{SC} exists only because of a non-zero α , and $\tilde{\Delta}_e$ is larger than Δ_e (Ref. 27), hence the gap along the two electron FSs has “accidental” nodes. Still, this is $s\pm$ superconductivity because Δ_h and Δ_e have opposite signs. As L increases, the SC vertex Γ evolves, according to Fig. 11, and eventually gets close to would be solution for $\alpha = 0$. For the latter, $\Delta_e = 0$, and the gap obviously has no nodes. The crossover from one limit to the other is displayed in Fig. 13, where we show the flow of the gaps Δ_h , Δ_e , and $\tilde{\Delta}_e$, corresponding to the leading SC vertex. For the value of α which we used in this figure ($\alpha = 0.4$) the transition from nodal to nodeless gap occurs at L smaller than the one at which SC vertex crosses the SDW vertex, i.e., when SC becomes the leading instability, the superconducting gap is already nodeless. But for other

values of α we can get either nodeless or nodal SC in this regime. In Fig. 14 we plot the “phase diagram” coming out of parquet RG for different α [the bare values of u_i are the same for all figures in this section]. In white region, SDW vertex is the largest and SC vertex is subleading [meaning that superconductivity can be revealed only by killing SDW order by doping]. In the shaded region the SC vertex is the largest. We see that superconducting gap in this region can actually be either nodal or nodeless, depending on the value of α .

C. RG flow below the scale of E_F

We now consider the situation below E_F . As in the 2-pocket model, we have to introduce three different u_3 couplings ($u_3^{(a)}$, $u_3^{(b)}$, and $u_3^{(c)}$) of which $u_3^{(b)}$ is the part of SDW vertex, and $u_3^{(c)}$ is the part of the SC vertex (the corresponding $u_3^{(i)}$ replace u_3 in Eqs. (17) and (18)). The flow of the couplings is now governed by

$$\begin{aligned} \dot{u}_5 &= - \left[u_5^2 + 2(u_3^{(c)})^2 \right] \\ \dot{\tilde{u}}_4 &= - \left[\tilde{u}_4^2 + 2(u_3^{(c)})^2 \right] \\ \dot{u}_1 &= + \left[u_1^2 + (u_3^{(b)})^2 \right] \\ \dot{u}_2 &= + \left[2u_1u_2 - 2u_2^2 \right] \\ \dot{u}_3^{(a)} &= 2u_1u_3^{(a)} - 2u_2u_3^{(a)} \\ \dot{u}_3^{(b)} &= 2u_1u_3^{(b)} \\ \dot{u}_3^{(c)} &= [u_5 + \tilde{u}_4] u_3^{(c)} \end{aligned} \quad (23)$$

Note the \tilde{u}_4 and u_5 have identical equations and hence treated identically. One can then straightforwardly verify using (20) that SC and SDW vertices decouple, as they should, and each satisfies $\dot{\Gamma}_i = \Gamma_i^2$. Hence, as before, whichever vertex is larger at E_F gives rise to the instability. If SC vertex prevails, the system becomes SC at perfect nesting and remains a SC at finite dopings. If SDW vertex prevails, the system becomes an SDW antiferromagnet at perfect nesting and then eventually becomes a SC upon doping. In distinction to the 2-pocket case, we don’t need to worry about the sign of the SC vertex once SDW instability is reduced by doping because one of Γ^{SC} is always attractive (see Fig. 11). We emphasize again that this attractive Γ^{SC} leads to either nodeless $s\pm$ gap, or to $s\pm$ gap with nodes along the electron FSs, depending on α and on the interplay between E_F and the scale at which parquet RG flow reaches the fixed point.

D. Summary of the results for the 3-band model

Collecting all the points we have discussed – we have shown that under suitable extent of renormalization of

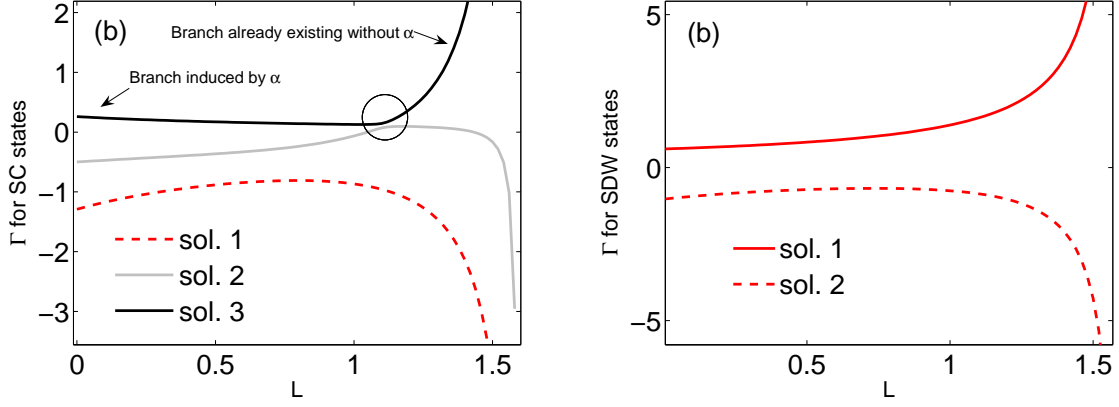


FIG. 11: The flow of SC and SDW vertices under RG in 3-pocket model for $\alpha = 0.4$. Panel (a) 3 SC vertices. One solution is attractive for all L (and corresponds to $s\pm$ pairing), the other two are repulsive. One of the repulsive solutions is of $s\pm$ character, another of $s++$ character. At small L , the positive solution is the one induced by α , at large L it almost coincides with the solution which becomes positive for these L already at $\alpha = 0$. The circle marks the area where positive and negative solutions come close to each other. The splitting between the two increases with α . (b) The two SDW vertices. One vertex is always attractive (positive) and the other is repulsive (negative).

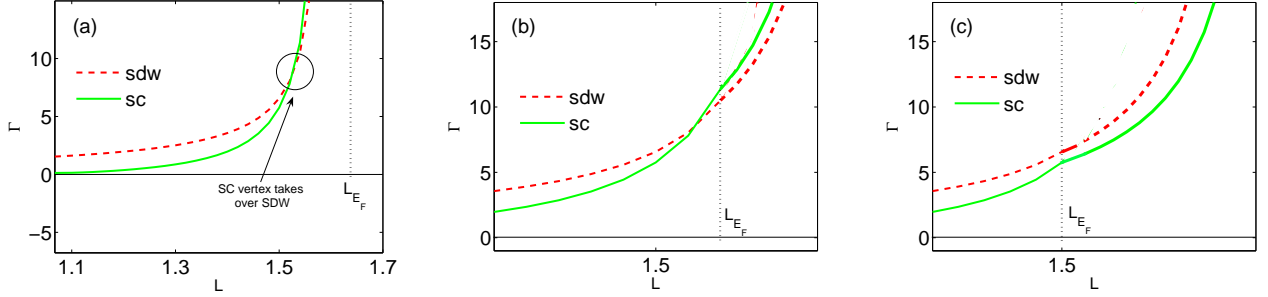


FIG. 12: The flow of vertices for different values of L_{EF} for $\alpha = 0.4$. (a) RG flow reaches fixed point before L_{EF} . SDW vertex is larger at small L , but SC vertex ‘crosses’ the SDW vertex at some distance from the fixed point and becomes the strongest vertex at the fixed point. As a result, the system develops a SC order. (b) L_{EF} is reached after the ‘crossing’ but before reaching fixed point. The system still develops a SC order, and SDW order does not emerge. (c) L_{EF} is reached before the ‘crossing’. In this case the SDW vertex still develops at small dopings, and SC order emerges at larger dopings, when SDW order gets suppressed.

the Coulomb repulsion and pair-hopping couplings one can have SDW, nodal $s\pm$, and nodeless $s\pm$ state even at perfect nesting. The angular dependence of the interaction between holes and electrons tends to drive the system towards a nodal SC phase. The SC order develops if the fixed point is reached within parquet RG, but if the scale E_F is reached before that, the system develops either SDW or SC order (either nodeless or nodal), depending on at what L the flow crosses over from parquet to ladder RG. That the SC $s\pm$ order can emerge even at perfect nesting is specific feature of the 3-pocket model. This feature was not present in the 2-pocket model, where the fixed point had an $O(6)$ symmetry. This symmetry is clearly broken in the 3-pocket model, even when $\alpha = 0$. The ‘crossing’ of the SDW and SC vertices can be unambiguously attributed to the presence of the other electron pocket because doing so helps SC but not SDW.

Fig. 15 summarizes the implication of our results towards the actual phase diagrams of Fe-pnictides. In the SDW dominated region (red), SC emerges after doping reduces SDW order. In the other part where SC dominates, SC order prevails already at perfect nesting. The $s\pm$ SC gap can be nodeless or have nodes along electron FSs depending on how strong is the angular dependence of the interaction between electrons and holes.

Before we exit this section, we would like to add two more comments regarding the 3-pocket model.

E. Effect of the angular dependence of e-e interaction

For completeness, we computed the evolution of the SC gap structure under RG flow for the case when we

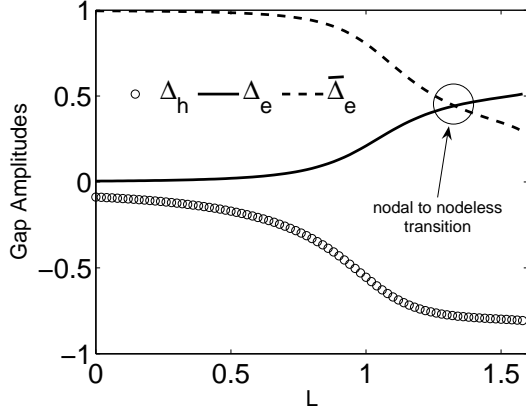


FIG. 13: The evolution of the three components of the superconducting gap with L for $\alpha = 0.4$. Δ_h is the gap on the hole FS, and $\Delta_e \pm \bar{\Delta}_e \cos 2\phi$ are the gaps along electron FSs. A circle marks the point where Δ_e and $\bar{\Delta}_e$ cross, and the gap along each of electron FSs changes from nodal to nodeless. Note that the solution is always of $s\pm$ character; meaning Δ_h and Δ_e are of opposite signs.

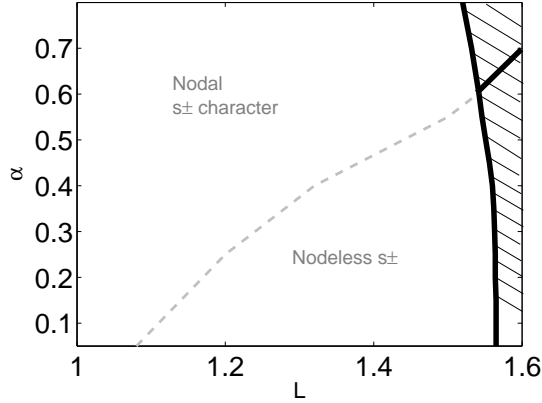


FIG. 14: The RG flow of the 3-pocket model in variables α and L over the range of energies above E_F . The white zone is where SDW vertex is the largest, and the shaded zone is where SC $s\pm$ vertex is the largest. The thick solid line in the shaded zone marks the transition from nodal to nodeless $s\pm$ gap in the region where SC vertex wins. The dashed line is the continuation of this transition line into the region where SDW vertex takes over.

preserve the angular dependence in the e-e interaction (u_4 term) in the form of Eq. (6). The set of equations for the SC vertices is now

$$\begin{pmatrix} 1 - u_5 L & -2u_3 L & -2\alpha u_3 L \\ -u_3 L & 1 - \tilde{u}_4 L & -\alpha \tilde{u}_4 L \\ -2\alpha u_3 L & -2\alpha \tilde{u}_4 L & 1 \end{pmatrix} \begin{pmatrix} \Delta_h^o \\ \Delta_e^o \\ \bar{\Delta}_e^o \end{pmatrix} = \begin{pmatrix} \Delta_h \\ \Delta_e \\ \bar{\Delta}_e \end{pmatrix} \quad (24)$$

As before, we need to diagonalize this set, cast the result in the form $\Delta_i = \Delta_i^o(1 + \Gamma_i L)$ and consider the largest Γ_i . The evolution with L of Δ_h , Δ_e , and $\bar{\Delta}_e$ for such Γ_i

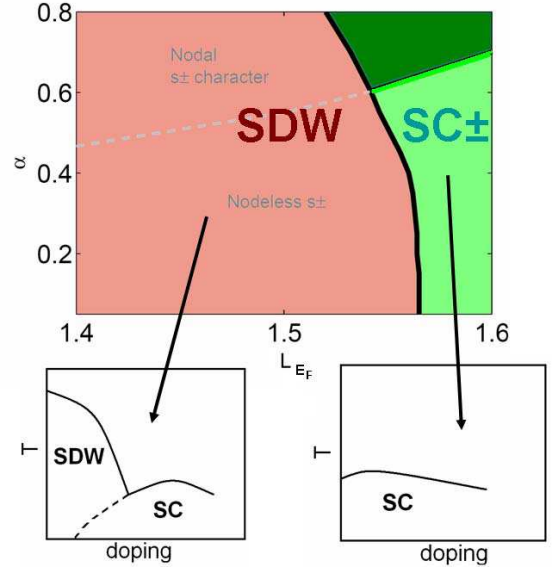


FIG. 15: The phase diagram of the 3-pocket model at perfect nesting in variables α and $L_{EF} = \log \Lambda/E_F$. In red is the region where SDW order develops, and in green is the region of the SC order. Dark and light green regions correspond to nodal (dark) and nodeless (light) SC gap along the electron FSs. The two sub-figures show the behavior at finite doping. Superconducting state which is brought out upon doping in the left sub-figure is either nodeless or nodal depending on the location with respect a dashed line inside the red (SDW) region. The transition between SDW and SC states can be either first order or involve intermediate co-existence phase^{46,47}.

is shown in Fig 16, and the phase diagram is shown in Fig. 17. The only change the angular dependence of u_4 brings in is that over some range when $\bar{\Delta}_e$ is the largest and the gap has nodes along the electron FSs, the gap actually has $s++$ character in the sense that Δ_h and Δ_e are of the same sign. But the character of the gap changes to $s\pm$ even before it becomes nodeless.

F. Role of Arsenic

The principle effect of As is to fold the BZ by doubling the unit cell area. To a certain extent, whether to work in the folded or unfolded zone is a matter of choice. But there is one qualitative difference between the two zones: some of the process that are not allowed in the unfolded zone are allowed in the folded zone as umklapp processes. An example of such process is shown in Fig. 18: two fermions from the hole band near $k = 0$ scatter into two fermions at two *different* electron pockets. In the unfolded zone, this process doesn't conserve momentum, and we didn't include it into our consideration. In the folded zone, both electron FSs are at (π, π) , and this process is an umklapp process. The difference is indeed due to the fact that in reality such process involves intermediate states on As.

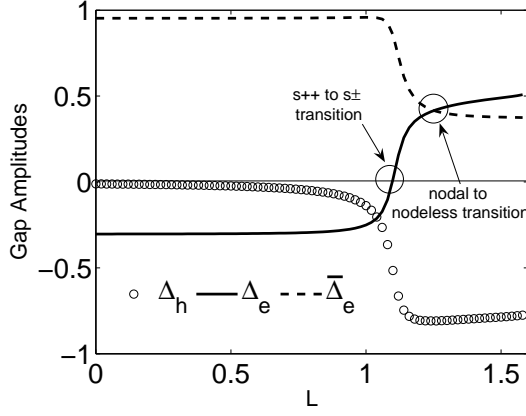


FIG. 16: Behavior of the different Δ 's when the angular dependence of the electron intra-pocket coupling u_4 is included. As before, we set $\alpha = 0.4$. The only difference compared to Fig. 13 is the appearance of the region, at small L , where SC order parameter has nodal $s++$ character meaning that Δ_h and Δ_e are of the same sign. In this range of L the SC vertex is, however, smaller than the SDW vertex. The character of the SC gap changes to $s\pm$ before SC vertex takes over SDW vertex.

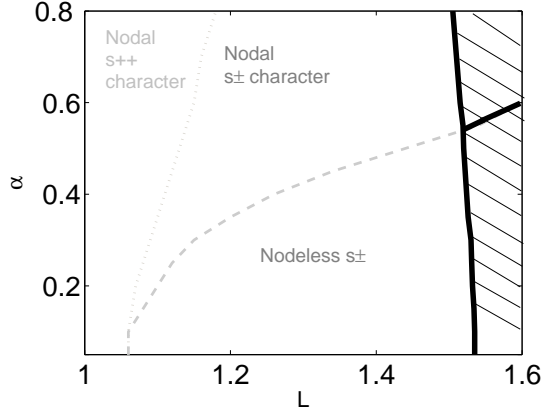


FIG. 17: Same as in Fig. 14, but with the angular dependence of the electron intra-pocket coupling u_4 included. The only new feature is the existence of a range where SC vertex (secondary in this range compared to SDW vertex) has nodal $s++$ character.

Neither our RG procedure nor fRG calculations include such terms. How important are they is not known. On general grounds, such interactions tend to enhance the SDW vertex and might potentially alter the picture that we presented. They also may alter the ordering momentum of the SDW state. This remains an open issue.

V. A 4-POCKET MODEL

We now extend the analysis from previous two sections to a 4-pocket model in which we include into consider-

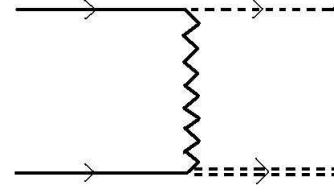


FIG. 18: The scattering which takes two fermions from the region near $k = 0$ and scatters them to fermions with momenta near $(\pi, 0)$ and $(0, \pi)$. This process is not allowed in the folded BZ because of momentum non-conservation, but it is allowed as an umklapp process in the folded BZ, which knows about As .

ation the additional hole pocket appearing at M point in the unfolded BZ. We remind that this model actually corresponds to 5-pocket model because we neglected for simplicity one of two hole pockets centered at $k = 0$.

The FS geometry and interactions contributing to the SC vertex are presented in Fig. 19

The Hamiltonian now contains three new terms u_9 , u_{10} , and u_{11} , which correspond to interactions between fermions belonging to two different hole pockets. In addition, we have three new vertices shown in shown in Fig. 20. These include fermions from two different hole and two different electron FSs. We call them w_i vertices (i runs from 1 to 3).

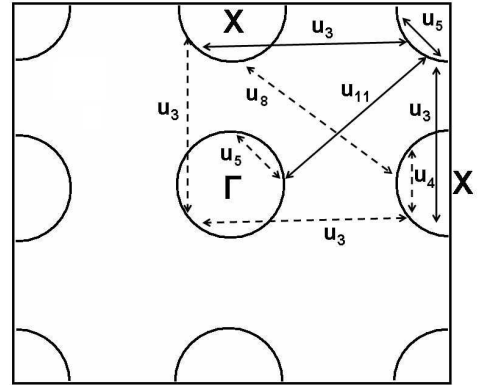


FIG. 19: The FSs and interactions in the 4-pocket model. Dashed lines mark the interactions already present in 3-pocket model, solid lines mark the new pairing interactions specific to 4-pocket model. As before, we only present interactions which contribute to the pairing vertices. There are other density-density and exchange interactions between electrons belonging to different pockets.

The Hamiltonian now has the form

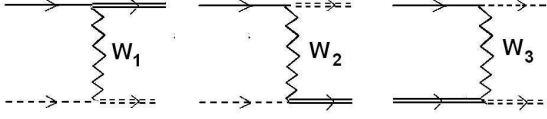


FIG. 20: The new interaction vertices for the 4-pocket model. Single and double solid lines denote fermions from the two hole pockets, single and double dashed lines denote fermions from the two electron pockets.

$$\begin{aligned}
\frac{m}{2\pi} H_{int} = & \sum u_1^{(1)} c_{1p_1s}^\dagger f_{1p_2s'}^\dagger f_{1p_4s'} c_{1p_3s} + \sum u_2^{(1)} c_{1p_1s}^\dagger f_{1p_2s'}^\dagger c_{1p_4s'} f_{1p_3s} + \sum \frac{u_3^{(1)}}{2} (c_{1p_1s}^\dagger c_{1p_2s'}^\dagger f_{1p_4s'} f_{1p_3s} + h.c.) \\
& + f_1 \leftrightarrow f_2 \text{ (with } c_1 \text{ unchanged) and } u_i^{(1)} \leftrightarrow u_i^{(2)} + c_1 \leftrightarrow c_2 \text{ (with } f_1 \text{ unchanged) and } u_i^{(1)} \leftrightarrow u_i^{(3)} \\
& + c_1 \leftrightarrow c_2 \text{ (with } f_2 \text{ unchanged) and } u_i^{(2)} \leftrightarrow u_i^{(4)} \\
& + \sum \frac{u_4^{(1)}}{2} f_{1p_1s}^\dagger f_{1p_2s'}^\dagger f_{1p_4s'} f_{1p_3s} + \sum \frac{u_4^{(2)}}{2} f_{2p_1s}^\dagger f_{2p_2s'}^\dagger f_{2p_4s'} f_{2p_3s} \\
& + \sum \frac{u_5^{(1)}}{2} c_{1p_1s}^\dagger c_{1p_2s'}^\dagger c_{1p_4s'} c_{1p_3s} + \sum \frac{u_5^{(2)}}{2} c_{2p_1s}^\dagger c_{2p_2s'}^\dagger c_{2p_4s'} c_{2p_3s} \\
& + \sum u_6 f_{1p_1s}^\dagger f_{2p_2s'}^\dagger f_{2p_4s'} f_{1p_3s} + \sum u_7 f_{1p_1s}^\dagger f_{2p_2s'}^\dagger f_{1p_4s'} f_{2p_3s} + \sum \frac{u_8}{2} (f_{1p_1s}^\dagger f_{1p_2s'}^\dagger f_{2p_4s'} f_{2p_3s} + h.c.) \\
& + c \leftrightarrow f \text{ and } (u_6, u_7, u_8) \leftrightarrow (u_9, u_{10}, u_{11}) \\
& + \sum w_1 c_{1p_1s}^\dagger f_{1p_2s'}^\dagger f_{2p_4s'} c_{2p_3s} + \sum w_2 c_{1p_1s}^\dagger f_{1p_2s'}^\dagger c_{2p_4s'} f_{2p_3s} + \sum \frac{w_3}{2} c_{1p_1s}^\dagger c_{2p_2s'}^\dagger f_{1p_4s'} f_{2p_3s} + (1 \leftrightarrow 2)
\end{aligned} \quad (25)$$

The u_4 's and u_5 's for all bands are treated on equal footing and hence $u_4^{(x)} = u_5^{(y)}$, $x, y = 1, 2$ and we just call them all u_4 .

The analysis of the 4-pocket model parallels that of the 3-pocket model, so we will be rather brief and only present the results.

A. The vertices

The SC and SDW vertices are obtained in the same way as before. We have (for $\alpha = 0$)-

$$\begin{aligned}
\Gamma^{SDW} &= \tilde{u}_1 + \tilde{u}_3 \\
\Gamma^{SC} &= \frac{-2(u_4 + u_5) + \sqrt{4(u_4 - u_5)^2 + 16u_3^2}}{2} \quad (26)
\end{aligned}$$

where $\tilde{u}_1 = u_1 + w_1$ and $\tilde{u}_3 = u_3 + w_3$ (see Fig. 21).

B. RG flow between Λ and E_F

The set of parquet RG equations is obtained in the same way as before. The couplings u_9 and u_{10} do not contribute to either Γ^{SC} or Γ^{SDW} and flow under RG independently of the couplings which do contribute to

either SC or SDW vertex, much like u_6 and u_7 terms. In line with previous analysis, we omit u_6 , u_7 , u_9 , and u_{10} terms. Further, the RG equations for u_4 , u_5 , u_8 and u_{11} are identical, and these four couplings tend to the same value at the fixed point. To make the presentation compact, we set $u_4 = u_5 = u_8 = u_{11}$ from the start and call them as u_4 . Collecting the equations for other variables we obtain

$$\begin{aligned}
\dot{u}_1 &= -[u_1^2 + u_3^2 + w_1^2 + w_3^2] \\
\dot{w}_1 &= -[2u_1w_1 + 2u_3w_3] \\
\dot{u}_2 &= [2u_1u_2 - 2u_2^2 - 2w_2^2 + 2w_1w_2] \\
\dot{w}_2 &= [2u_1w_2 + 2w_1u_2 - 4u_2w_2] \\
\dot{u}_3 &= 4u_1u_3 - 2u_2u_3 - 4u_4u_3 + 4w_1w_3 - 2w_2w_3 \\
\dot{w}_3 &= 4u_1w_3 + 4u_3w_1 - 2u_2w_3 - 2u_3w_2 - 4u_4w_3 \\
\dot{u}_4 &= [2u_4^2 + 2u_3^2] \quad (27)
\end{aligned}$$

Analyzing these equations, we find that the combinations $u_1 - w_1$ and $u_2 - w_2$ which do not contribute to either Γ^{SDW} or Γ^{SC} decouple from other equations. As before, we assume that the bare values of the couplings are such that there no pre-emptive instability before SDW and SC ones and neglect these three combinations. For the rest we introduce $\tilde{u}_1 = u_1 + w_1$, $\tilde{u}_3 = u_3 + w_3$ and $\tilde{u}_2 = u_2 + w_2$, and re-express the first five equations in Eq. 27 as

C. RG flow below the scale of E_F

$$\begin{aligned}
 \dot{\tilde{u}}_1 &= -[\tilde{u}_1^2 + \tilde{u}_3^2] \\
 \dot{\tilde{u}}_2 &= [2\tilde{u}_1\tilde{u}_2 - 2\tilde{u}_2^2] \\
 \dot{\tilde{u}}_3 &= 4\tilde{u}_1\tilde{u}_3 - 2\tilde{u}_2\tilde{u}_3 - 4u_4\tilde{u}_3
 \end{aligned}
 \tag{28}$$

Solving this set Eqs. 27 and 28 and substituting the results into the expressions for the largest Γ^{SC} and Γ^{SDW} , we find the flow of the vertices. We show the results in Fig. 22. This figure shows that the system behavior in a 4-pocket model is “intermediate” between 2-pocket and 3-pocket models. On one hand, like in a 3-pocket model, the largest SC vertex is always positive, i.e., there is no critical L before which SC vertex is repulsive. The implication is that the system always becomes a SC when the competing SDW instability is reduced. The SC gap is either nodeless or with nodes on electron FSs, depending on α , much like in the unshaded region in Fig. 14. On the other hand, like in a 2-pocket model, SDW vertex remains larger than SC vertex for all L before the fixed point is reached, and the two vertices flow to the same value at the fixed point (Fig. 22). This similarity with a 2-pocket model was first noted by K. Haule⁴⁸ and can be understood if we note that in the 4 pocket case SC pairing is the same as in 3-pocket model (with extra combinatoric factor of 2 compared to 2-pocket case), but SDW pairing is now possible between the two sets of e-h pockets (see Fig. 21), this adds the combinatoric factor of 2 also to the renormalization of the SDW vertex.

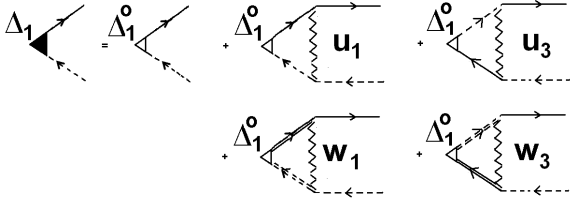


FIG. 21: The diagrammatic equation for the renormalized SDW vertex in the 4-pocket model. Comparing with the corresponding Fig. 8)a for the 3-pocket case, there are extra diagrams which contribute to the SDW vertex. This leads to effectively doubling Γ^{SDW} .

That SDW and SC vertices flow to the same value at the fixed point of parquet RG (and, hence, the fixed point has a higher symmetry) once we add an additional hole pocket at (π, π) follows from the numerical solution of the fRG equations by Thomale et al.²⁶. Our analytical RG results for this case again agree with their fRG, which, in our opinion, is another confirmation that the “topology” of the RG flow is chiefly determined by combinatoric effects.

The system behavior for the case when the fixed point of the functional RG is not reached at $E > E_F$ is quite similar to the 2-pocket model with the only difference that now SC instability always occurs when SDW order is destroyed by doping. Namely, at perfect nesting the system develops SDW order. At finite doping, the RG flow of the SDW vertex levels off, and SC vertex eventually becomes larger. The SC gap has \pm structure either without or with nodes along the electron FS, depending on the values of α and of $\log \Lambda/E_F$. The phase diagram is line in Fig. 15, but with only “SDW” region.

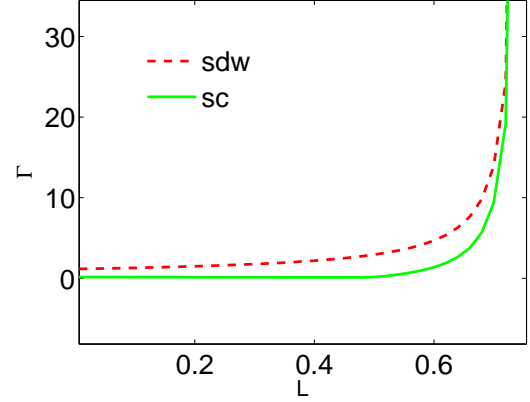


FIG. 22: Parquet RG flow of SC and SDW vertices for the 4-pocket model at $\alpha = 0.3$. The SDW vertex remains the largest over the whole flow, and the ratio of the SDW and SC vertices approaches one at the fixed point of parquet RG. This is very similar to the 2-pocket case except that here Γ^{SC} is attractive for all L .

VI. CONCLUSION

We have done calculations addressing on the same footing the issues of the interplay between intra and inter-pocket Coulomb repulsion in the Fe-based superconductors, the competition between SC and SDW orders, and the angular dependence of the SC gap. We considered a toy 2-pocket model (one hole and one electron pocket), and more realistic models of two electron pockets and either two or three hole pockets. We neglected the hole pocket centered at $k = 0$, which is less nested with the electron pockets than the other hole pocket at $k = 0$, and ended up with 3-pocket and 4-pocket models. We considered the flow of the couplings and SC and SDW vertices within analytical parquet RG scheme. Fluctuations in the SDW and SC channels are coupled at intermediate energies $\Lambda > E > E_F$, but decouple at energies below E_F . The system behavior below E_F is governed by conventional ladder RG, when each vertex flows according to $d\Gamma_i/dL = \Gamma_i^2$.

For the toy 2-pocket model, earlier results show^{21,43} that SDW instability is the dominant one at perfect nesting. The SC vertex is repulsive at large energies but changes sign under parquet RG and become attractive above some RG scale. The SDW and SC couplings flow to the same value at the fixed point of RG equations, and the fixed point of parquet RG has extended $O(6)$ symmetry. If the scale of E_F is reached before this fixed point, SDW order prevails at zero doping but is reduced and eventually destroyed at finite doping. Whether or not SC appears in place of SDW order depends on whether SC vertex already changes sign and becomes attractive at E_F . If superconductivity appears, the SC gap has a simple plus-minus structure.

The main goal of this paper was to understand how this scenario is modified in realistic 3-pocket and 4-pocket models. Our main results are the following:

- In both 3-pocket and 4-pocket models electron-hole and electron-electron interactions are generally angle dependent. The most relevant angle dependence is in the form $\cos 2\phi$, where ϕ is the angle along one of electron FSs. Because of this angular dependence, there are three different vertices in the SC channel. One of these vertices turns out to be attractive at all scales. The symmetry of the attractive interaction is extended s -wave. Other two SC vertices are repulsive.
- This attractive SC vertex favors the $s\pm$ state in which the gaps along hole FSs are angle-independent (up to $\cos 4\phi$ corrections), while the gaps along the two electron FSs are in the form $\Delta_e \pm \bar{\Delta}_e \cos 2\phi$. The interplay between Δ_e and $\bar{\Delta}_e$ depends on the strength of $\cos 2\phi$ component of the interaction and also on the interplay between intra-pocket and inter-pocket Coulomb repulsions. Depending on the parameters, the electron gaps can be either nodeless ($\Delta_e > \bar{\Delta}_e$), or have accidental nodes ($\Delta_e < \bar{\Delta}_e$).
- In 4-pocket model at perfect nesting, the SDW vertex remains larger than this attractive SC vertex. The two flow up to the same values at the fixed point, if this fixed point is at an energy larger than E_F . Then the system cannot distinguish between SC and SDW. If the system flows down to E_F without yet reaching the fixed point, SDW order wins.

Away from perfect nesting, SDW order is reduced and the system eventually develops a SC instability

- In 3-pocket model, the situation is generally similar, but before the fixed point of parquet RG is reached, SC vertex becomes larger than SDW vertex. If this happens before the scale of E_F is reached, the system develops SC instability already at perfect nesting, and SDW instability does not appear. If SDW vertex remains the largest down to E_F , the system develops SDW instability at and around perfect nesting, and SC instability at larger dopings.

The results for the 3-pocket case demonstrate that SDW order need not be the pre-requisite to $SC\pm$ order, also for most part of the phase diagram it does appear at perfect nesting, and SC only appears upon doping. We also emphasize that the interplay between SC and SDW is both “mutual support” and “competition”. Namely, SC and SDW *fluctuations* tend to enhance each other, what is relevant is the fact that in the applicability range of parquet RG (when SC and SDW fluctuations talk to each other), both SC and SDW vertices diverge upon approaching the fixed point. At the same time, SDW and SC *orders* compete with each other^{46,47}, meaning that SC order only emerges when SDW order is reduced enough by doping, and SDW order does not emerge at all if SC order emerges first already at perfect nesting.

We also emphasize that our analytical results are fully consistent with numerical fRG study of these models. We view this agreement as the evidence that most of the physics of multi-pocket *Fe*-pnictides is captured within simplified 3-pocket or 4-pocket low-energy models.

Acknowledgements

We acknowledge helpful discussions with L. Benfatto, R. Fernandes, W. Hanke, P. Hirschfeld, I. Eremin, Y. Matsuda, I. Mazin, R. Prozorov, D. Scalapino, J. Schmalian, Z. Tesanovic, R. Thomale, M. Vavilov, and A. Vorontsov. This work was supported by NSF-DMR-0906953. Partial support from MPI PKS (Dresden) (S.M. and A.V.C), Ruhr-University Bochum (S.M), and Humboldt foundation (A.V.C) is gratefully acknowledged.

¹ Y. Kamihara, T. Watanabe, M. Hirano, H. Hosono, J. Am. Chem. Soc. **130**, 3296(2008).

² X. H. Chen, T. Wu, G. Wu, R. H. Liu, H. Chen, D. F. Fang, Nature **453**, 761(2008).

³ G. F. Chen, Z. Li, D. Wu, G. Li, W. Z. Hu, J. Dong, P. Zheng, J. L. Luo, and N. L. Wang, Phys. Rev. Lett. **100**, 247002 (2008).

⁴ Z.-A. Ren, *et. al.*, Europhys. Lett. **83**, 17002(2008)

⁵ M. Rotter, M. Tegel, D. Johrendt, Phys. Rev. Lett. **101**, 107006 (2008)

⁶ K. Sasmal, B. Lv, B. Lorenz, A. M. Guloy, F. Chen, Y.-Y. Xue, and C.-W. Chu, Phys. Rev. Lett. **101**, 107007 (2008),

⁷ N. Ni, A. Thaler, J. Q. Yan, A. Kracher, E. Colambier, S. L. Bud'ko, P. C. Canfield, Phys. Rev. B **82**, 024519 (2010).

⁸ X. C. Wang, *et. al.*, arXiv:0806.4688v3; S.V, Borisenko *et al* Phys. Rev. Lett. **105**, 067002 (2010).

- ⁹ Y. Mizuguchi, F. Tomioka, S. Tsuda, T. Yamaguchi, and Y. Takano, Appl. Phys. Lett. **93**, 152505 (2008), F. C. Hsu et al., Proc. Natl. Acad. Sci. U.S.A. **105**, 14 262 (2008), M. H. Fang et al., Phys. Rev. B **78**, 224503 (2008), G. F. Chen et al., Phys. Rev. B **79**, 140509(R) (2009), B. Zeng et. al., arXiv:1007.3597.
- ¹⁰ C. de la Cruz et. al., Nature, **453**, 899 (2008). For the latest results on magnetic measurements, see D. S. Inosov, et. al., Nature Physics **6**, 178-181 (2010) and references therein.
- ¹¹ Y. Kamihara et al., J. Am. Chem. Soc. **128**, 10012 (2006).
- ¹² M. Li et. al. Phys. Rev. B **80**, 024515 (2009)
- ¹³ S.E. Sebastian et. al., J. Phys.: Condens. Matter **20** 422203(2008).
- ¹⁴ D.J. Singh and M.-H. Du, Phys. Rev. Lett. **100**, 237003 (2008); M.J. Calderon, B. Valenzuela, and E. Bascones, Phys. Rev. B **80**, 094531 (2009).
- ¹⁵ L. Boeri, O. V. Dolgov, and A. A. Golubov, Phys. Rev. Lett. **101**, 026403 (2008)
- ¹⁶ I. I. Mazin, D. J. Singh, M. D. Johannes, and M. H. Du, Phys. Rev. Lett. **101**, 057003 (2008)
- ¹⁷ K. Kuroki, H. Usui, S. Onari, R. Arita, and H. Aoki, Phys. Rev. B **79**, 224511 (2009).
- ¹⁸ Seiichiro Onari and Hiroshi Kontani, arXiv:1009.3882.
- ¹⁹ K. Seo, B. A. Bernevig, and J. Hu, Phys. Rev. Lett. **101**, 206404 (2008)
- ²⁰ K. Kuroki et. al., Phys. Rev. Lett. **101**, 087004 (2008)
- ²¹ A. V. Chubukov, D. V. Efremov, and I. Eremin, Phys. Rev. B **78**, 134512 (2008)
- ²² V. Stanev, J. Kang, Z. Teseanovic, Phys. Rev. B **78**, 184509 (2008); V. Stanev, B. S. Alexandrov, P. Nokolić, Z. Tešanović, arXiv:1006.0447.
- ²³ S. Graser, T. A. Maier, P. J. Hirschfeld, D. J. Scalapino, New J. Phys. **11**, 025016 (2009).
- ²⁴ Fa Wang et. al., Phys. Rev. Lett. **102**, 047005 (2009).
- ²⁵ C. Platt, C. Honerkamp, and Werner Hanke, New J. Phys. **11**, 055058 (2009). ; R. Thomale et. al., Phys. Rev. B **80**, 180505 (2009).
- ²⁶ R. Thomale, C. Platt, W. Hanke, B. A. Bernevig, arXiv:1002.3599v1
- ²⁷ A. V. Chubukov, M. G. Vavilov, A. B. Vorontsov, Phys. Rev. B **80**, 140515(R)(2009).
- ²⁸ A. F. Kemper, T. A. Maier, S. Graser, H.-P. Cheng, P. J. Hirschfeld, and D. J. Scalapino, New J. Phys. **12**, 073030 (2010).
- ²⁹ S. Graser, A. F. Kemper, T. A. Maier, H.-P. Cheng, P. J. Hirschfeld, and D. J. Scalapino, Phys. Rev. B **81**, 214503 (2010).
- ³⁰ Y. Nakai, et. al., J. Phys. Soc. Jpn. **77**, 073701 (2008)
- ³¹ H.-J. Grafe, et. al., Phys. Rev. Lett. **101**, 047003 (2008)
- ³² Y. Wang, et. al., Supercond. Sci. Technol. **22** 015018(2009).
- ³³ O. Millo, et. al. Phys. Rev. B **78**, 092505 (2008)
- ³⁴ J. D. Fletcher et. al., Phys. Rev. Lett., **102**, 147001(2009)
- ³⁵ C. W. Hicks et. al., Phys. Rev. Lett., **103**, 177003(2009)
- ³⁶ K. Hashimoto et. al., Phys. Rev. B **81**, 220501(R) (2010)
- ³⁷ K. Hashimoto et. al., Phys. Rev. Lett. **102**, 017002 (2009)
- ³⁸ L. Malone et. al., Phys. Rev. B **79**, 140501(R) (2009)
- ³⁹ H. Ding et. al., Europhys. Lett., **83**, 47001(2008).
- ⁴⁰ Seiichiro Onari and Hiroshi Kontani, Phys. Rev. Lett. **103**, 177001 (2009).
- ⁴¹ W. L. McMillan, Phys. Rev. **167**, 331 (1968); N.N. Bogolubov, V.V. Tolmachev, and D.V. Shirkov, Consultants Bureau, 1959.
- ⁴² I. Mazin and J. Schmalian, Physica C, **469**, 614 (2009)
- ⁴³ A. V. Chubukov Physica C **469**, 640(2009).
- ⁴⁴ D. J. Singh, Phys. Rev. B, **78**, 094511(2008).
- ⁴⁵ I. Eremin and A.V. Chubukov, Phys. Rev. B **81**, 024511 (2010).
- ⁴⁶ R. M. Fernandes and J. Schmalian, Phys. Rev. B **82**, 014521 (2010)
- ⁴⁷ A.B.Vorontsov, M.G.Vavilov, and A.V.Chubukov, Phys. Rev. B **81**, 174538 (2010); M. G. Vavilov, A. V. Chubukov, and A. B. Vorontsov, Supercond. Sci. Technol. **23**, 054011 (2010).
- ⁴⁸ K. Haule, unpublished.